



HAL
open science

Thermal and chemical enhanced recovery of heavy chlorinated organic compounds in saturated porous media: 1D cell drainage-imbibition experiments

Stéfan Colombano, Hossein Davarzani, E.D. van Hullebusch, D. Huguenot, Dominique Guyonnet, Jacques Deparis, Ioannis Ignatiadis

► To cite this version:

Stéfan Colombano, Hossein Davarzani, E.D. van Hullebusch, D. Huguenot, Dominique Guyonnet, et al.. Thermal and chemical enhanced recovery of heavy chlorinated organic compounds in saturated porous media: 1D cell drainage-imbibition experiments. *Science of the Total Environment*, 2020, 706, pp.135758. 10.1016/j.scitotenv.2019.135758 . hal-02859913

HAL Id: hal-02859913

<https://brgm.hal.science/hal-02859913>

Submitted on 7 Mar 2022

HAL is a multi-disciplinary open access archive for the deposit and dissemination of scientific research documents, whether they are published or not. The documents may come from teaching and research institutions in France or abroad, or from public or private research centers.

L'archive ouverte pluridisciplinaire **HAL**, est destinée au dépôt et à la diffusion de documents scientifiques de niveau recherche, publiés ou non, émanant des établissements d'enseignement et de recherche français ou étrangers, des laboratoires publics ou privés.



Distributed under a Creative Commons Attribution - NonCommercial 4.0 International License

1
2
3
4
5
6
7
8
9
10
11
12
13
14
15
16
17
18
19
20
21
22
23
24
25
26

Abstract

Chemical and thermal enhanced recovery of pure heavy chlorinated organic compounds (DNAPL; dense non-aqueous phase liquids) were investigated by using lab-scale 1D cells. Temperature was increased to reduce DNAPL viscosity (and hence increase its mobility), while surfactant was added to decrease capillary forces involved in the entrapment of DNAPL in porous media. Laboratory scale experiments, based on mass balance and indirect monitoring methods (*i.e.*, permittivity, electrical resistivity and optical density), were conducted to quantify the effects of these enhancements. Heating the DNAPL up to 50 °C decreased its viscosity by a factor of two. The addition of a surfactant; *i.e.*, Sodium Dodecyl Benzene Sulfonate (SDBS), at its Critical Micelle Concentration (to prevent DNAPL solubilization), decreased interfacial tensions by a factor of 12. Drainage-imbibition experiments performed in 1D cells provided retention curves (capillary pressure as a function of water saturation) of a two-phase (DNAPL-water) system in experimental glass bead porous media. The observed reduction of residual saturation (S_m) obtained with SDBS was 28% for 0.5 mm-diameter glass beads (GB) and 46% for 0.1 mm GB. No significant decrease in S_m was observed with thermal enhancement. The van Genuchten – Mualem model was found to satisfactorily reproduce the measured retention curves. Indirect measurements of water saturations (S_w) showed that: i. measured permittivities were very close to values modeled with the Complex Refractive Index Model (CRIM); ii. Archie's Law was less successful in reproducing measured electrical resistivities; iii. optical densities provide accurate estimations of S_w . At field scale, the combined monitoring of electrical resistivity (which provides a global picture) and permittivity (which yields locally precise but spatially limited information) is expected to significantly improve the collection of information on residual saturations S_m .

27

28 **Keywords**

29

30 Dense Non-Aqueous Phase Liquids, chemical enhancement, thermal enhancement,
31 permittivity, electrical resistivity, optical density

32

33

34 **1. Introduction**

35 Chlorinated Organic Compounds (COCs) have been produced in large quantities since the middle
36 of the 20th century, mostly for chemical, pharmaceutical and agricultural applications [Cohen and
37 Mercer (1993); Kueper et al. (2003)]. Due to their high hydrophobicity and their density higher than
38 that of water, COCs may infiltrate aquifers vertically and form DNAPL (Dense Non-Aqueous Phase
39 Liquid) pools [Schwille (1988); Cohen and Mercer (1993)]. Their dispersion (by solubilization and
40 volatilization) from the pollution source zone may generate large contaminant plumes leading to
41 severe groundwater contamination [Stupp and Paus (1999)]. These particularly toxic pollutants, may
42 permanently affect soil, indoor air and groundwater quality [ADEME and Ernst & Young (2014);
43 NIEHS (2015); IARC (2018)].

44 Treating such contaminant sources is therefore a priority in order to avoid the migration of DNAPL
45 to groundwater over very long periods of time, leading to a buildup of contaminant plume
46 concentrations and plume spreading [Sale (2001); Stroo et al. (2003); Falta et al. (2005a); Falta et al.
47 (2005b); McDade et al. (2005); Newell and Adamson (2005); McGuire et al. (2006); Huang et al.
48 (2015)].

49 The recovery of COC free-phase (mobile) product is typically performed using pump and treat
50 methods. Due to COC high density, low solubility and strong interfacial tension with water, pump and
51 treat operations are time-consuming (*e.g.*, commonly in excess of 30 years). They are also not very
52 effective in the long term due to the slow release from the residual saturation and the low remediation
53 yield [Mackay and Cherry (1989); Travis and Doty (1990); Berglund and Cvetkovic (1995); Pankow
54 and Cherry (1996); Falta et al. (2005b); McDade et al. (2005); McGuire et al. (2006); Harkness and
55 Konzuk (2014)]. Typical recovery yields following pumping do not exceed 60% [ITRC (2002); Stroo
56 et al. (2012)]. DNAPL mobilization only starts when the sum of viscous and buoyancy forces exceed
57 capillary forces within the contaminated medium [Pennell et al. (1996); Duffield and Ramamurthy
58 (2003)].

59 The DNAPL studied herein was sampled from the subsurface of the Tavaux site; a large chloralkali
60 chemical plant located in the center-east of France. It is a mixture composed mainly of heavy

61 chlorinated organic compounds (weight percent; wt%): hexachlorobutadiene-HCBD (58%),
62 hexachloroethane-HCA (14%), perchloroethylene-PCE (8%), and pentachlorobenzene (3.5%), carbon
63 tetrachloride (4%), trichloroethylene-TCE (2%), hexachlorobenzene (1%) [Cazaux et al. (2014)]. Due
64 to the accidental release of DNAPL, the subsurface of the Tavaux site is contaminated, with locally
65 pure DNAPL present below the water table. Investigations aim therefore at optimizing the recovery of
66 this free phase, either through thermal (heating) or chemical (surfactants) enhancements.

67 Surfactants addition aims to: a) decrease the interfacial tension (IFT) between the organic phase
68 and water and b) increase NAPL solubility in water through micelle generation. Dissolution of
69 contaminants into micelles arises when surfactant concentrations exceed the Critical Micelle
70 Concentration (CMC) value in the pores [Rosen (1989)]. While the chlorinated compounds that are the
71 most documented in the literature are PCE and TCE, the DNAPL investigated in the present study
72 does not contain more than 15% (wt%) of these compounds. Also, there is a paucity of literature
73 regarding the main compounds encountered on the Tavaux DNAPL (*i.e.*, HCB and HCA). Nonionic
74 surfactants are effective for remediating chlorinated solvents such as PCE and TCE because of their
75 ability to reduce the IFT and increase pollutant solubility [Taylor et al. (2001); Zhong et al. (2003);
76 Zhao et al. (2006); Suchomel et al. (2007); Harendra and Vipulanandan (2011); Atteia et al. (2013);
77 Pennell et al. (2014)]. Several surfactants (*i.e.*, Triton X-100, Tween 80, Aerosol MA-80 and SDBS)
78 are able to solubilize and reduce the IFT for the TCE-water and PCE-water systems. For TCE, IFT has
79 been reduced from 35.2 to 0.2 mN.m⁻¹ with Aerosol-MA-80 [Dwarakanath et al. (1999)] and from 35.2
80 to 10.4 mN.m⁻¹ with Tween 80 [Suchomel et al. (2007)]. For PCE, the system's IFT can be reduced by
81 the Aerosol family of surfactants: from 47.8 to less than 0.01 mN.m⁻¹ [Dwarakanath et al. (1999);
82 Sabatini et al. (2000); Childs et al. (2004)], or by Triton X-100 and Tween 80 [Taylor et al. (2001);
83 Harendra and Vipulanandan (2011)]. In this work, the surfactants were introduced at concentrations
84 well below their respective CMC concentrations, in order to avoid DNAPL dissolution and hence the
85 need for costly water treatment technologies [Sabatini et al. (1998); Ahn et al. (2008); Atteia et al.
86 (2013); Maire et al. (2018)].

87 Regarding temperature enhancement, it has been shown that the viscosity of a chlorinated solvent is
88 generally reduced by 1% per degree Celsius incremental increase [Davis (1997)]. [Sleep and Ma

89 (1997)] observed a significant viscosity reduction with increasing temperature in the case of PCE.
90 Such viscosity reduction increases DNAPL mobility and therefore decreases residual saturations. She
91 and Sleep (1998) reported that increasing the temperature decreased residual PCE [She and Sleep
92 (1998)]. Kong (2004) also demonstrated during imbibition-drainage experiments that residual coal tar
93 saturations reduced when temperatures were increased from 22 to 50 °C (respectively $S_m = 31.4\%$ to
94 27.6% in F-70 sand and $S_m = 32.8\%$ to 21.8% in 20-30 mesh Ottawa sand) [Kong (2004)]. Indirect
95 monitoring of these residual saturations can be performed using several methods.

96 Permittivity measurements using Time-Domain Reflectometry (TDR) probes have served as
97 indicators of Dense Non-Aqueous Phase Liquid (DNAPL) saturation (S_n) [Redman et al. (1991);
98 Redman and DeRyck (1994); Kueper et al. (1993); Brewster et al. (1995)]. PCE samples spiked at
99 controlled values of saturation were monitored by TDR, with results showing a good correlation
100 between PCE saturation and permittivity interpreted using a mixing model [Redman and DeRyck
101 (1994)]. The most commonly used model for correlating dielectric permittivity to saturation levels in a
102 soil made of a mixture of particles, water and air, is the Complex Refractive Index Model (CRIM)
103 [Birchak et al. (1974); Roth et al. (1990); Endres and Knight (1992); Ajo-Franklin et al. (2004)].
104 Electrical resistivity is another parameter used as a means to estimate DNAPL saturation levels.
105 Interpretation is performed using Archie's Law, which describes how resistivity depends on porosity if
106 ionic conduction in the pore fluid dominates other conduction mechanisms in the rocks [Archie
107 (1942)]. Resistivity is described as the sum of a bulk conductivity term and a surface conductivity
108 term, both of which are saturation-dependent [Revil (2012)].

109 Finally, the Light Reflection Method (LRM) was used to calibrate NAPL saturation with optical
110 density [Alazaiza et al. (2016)]. Schincariol and Schwartz (1990) and Schincariol *et al.* (1993)
111 published the first studies showing a correlation between a reflected optical image and dyed NaCl
112 concentrations during miscible experiments [Schincariol and Schwartz (1990); Schincariol et al.
113 (1993)]. Flores *et al.* (2011) quantified the residual saturation of LNAPL using Sudan III dyed
114 (synthetic organic compounds) with brilliant blue FCF and Simplified Image Analysis Method
115 (SIAM). The difference between mass balance and image interpretation was only 4.7% [Flores et al.
116 (2011)]. O'Carroll *et al.* (2004) used LRM to estimate the saturation of tetrachloroethylene (PCE) in a

117 flow chamber and observed a linear relationship between the hue and PCE saturation (with a
118 correlation R^2 value of 0.91) [O'Carroll et al. (2004)]. Luciano *et al.* (2010) used mass balance
119 calculations to validate the suitability of LRM, with a difference between mass balance and image
120 interpretation of 6% [Luciano et al. (2010)]. Unlike previous authors, the approach adopted herein
121 relied on a calibration based on a superior number (4) of water saturation calibration points ($S_w = 0\%$,
122 100% , $1-S_{rm}$, and S_{rw}).

123 The purpose of this study was to assess the potential of chemical and thermal enhancements for
124 improving DNAPL recovery during pumping. Investigations were performed at lab scale with
125 controlled 1D cells, a DNAPL mixture collected in the field and porous media made of glass beads.
126 This experimental setup helped avoid potential artefact effects associated with porous medium
127 heterogeneity, while focusing on primary mechanisms and parameters (*e.g.*, interfacial tension,
128 micellar concentrations, ...) and on the indirect measurement of DNAPL saturation levels using three
129 different methods (permittivity, electrical resistivity and optical density).

130

131 **2. Materials and methods**

132 The DNAPL used for the experiments was sampled at the Tavaux site (June 25, 2014) and stored in
133 a cold room (at 4 °C). DNAPL was filtered just before its use (EMD Millipore, 0.45 μm). The water
134 used for all experiments was BRGM tap water degassed using an ultrasound tank (VWR Ultrasonic
135 Cleaner - USC500D: 60 °C, 45 Hz, 60 min). This tap water is extracted from a groundwater well that
136 shows very stable chemical characteristics.

137 The experiments with thermal enhancement were carried out in the 20-50 °C temperature range (in
138 order to avoid DNAPL volatilization). Four surfactants were tested at their CMC: 2 non-ionic (Triton
139 X-100: 4-(1,1,3,3-Tetramethylbutyl)phenyl-polyethylene glycol and Tween 80: sorbitan mono-9-
140 octadecenoate poly(oxy-1,2-ethanediyl)) and 2 anionic (Aerosol MA-80: sodium 1,4-dicyclohexyl
141 sulphonatosuccinate and SDBS: sodium dodecyl benzene sulfonate). All surfactants were supplied by
142 Sigma Aldrich (laboratory grade), except for the Aerosol MA-80, which was supplied by Cytec.

143

144 2.1 *Characterization of fluid physical properties*

145 All measurements presented herein were carried out in triplicate. Viscosity was first measured by
146 Rheonova Laboratory (Grenoble, France) using a Discovery Hybrid Rheometer - DHR 3 (TA
147 Instruments) and then at BRGM with a Haake Mars III rheometer from Thermo Fischer Scientific.
148 Measurements were performed at atmospheric pressure and at 10, 15, 20, 30, 45 and 60 °C.
149 Temperature was controlled through the Peltier effect. The temperature precision was 0.5 °C.

150 The IFT and contact angle between the DNAPL and water were measured at the Navier laboratory
151 (Champs-sur-Marne, France) with a Tracker-S tensiometer (Teclis Scientific) and also at BRGM with
152 a Drop Shape Analyser tensiometer DSA-100 (Krüss). The Tracker-S and the DSA-100 are automated
153 drop tensiometers that can measure variations in IFT over time. The instrument can also be used to
154 measure the contact angle between a liquid and a solid. Using optional lenses, the accuracy of IFT
155 measurement can be increased to 0.1 mN.m⁻¹. The IFT and contact angle for DNAPL-water were
156 measured at different temperatures (10 to 60 °C) and with surfactants at different concentrations. The
157 temperature was stabilized with a thermostatically controlled water bath. Product densities were
158 measured by first weighing three different 100 mL flasks and then weighing, for each temperature, the
159 product was weighed in the closed vial while adjusting the volume required to fill the flasks.

160

161 2.2 *Solubilization*

162 DNAPL solubility measurements were performed using the experimental protocol of Rodrigues *et*
163 *al.* (2017). The same protocol was applied for solubilization experiments in the presence of
164 surfactants. Four surfactant concentrations were studied, according to their respective CMC value,
165 from 0.25×CMC to 8×CMC. All measurements were performed in triplicate at 20 °C [Rodrigues *et al.*
166 (2017)].

167 COC concentrations in water were analyzed by gas chromatography with flame ionization detector
168 (Varian 3800) and head space injection (Agilent 7697A). The column used was an Agilent CP-SIL 5
169 CB (semi-capillary column, fused silica tube, length: 50 m, internal diameter: 0.53 mm, active phase:
170 polydimethylsiloxane, carrier gas: helium).

171

172 2.3 *Drainage-imbibition experiments in 1D cells*

173 The main objective of the experimental study was to characterize the soil parameters in two-phase
174 flow conditions (DNAPL and water) in a porous medium and under different conditions (thermal or
175 chemical enhancement). To achieve this objective, the laboratory work was dedicated to performing
176 drainage-imbibition experiments in 1D cells (filled with glass beads; GB) that were used to generate
177 the capillary pressure-saturation curves in static flow conditions. The 1D cells had an internal diameter
178 of 5.8 cm and a height of 5.56 cm (Figure 1). Two sizes of GB were used to fill the cells in order to
179 reproduce the hydraulic conductivities measured at the site: 0.10 ± 0.02 mm and 0.5 ± 0.1 mm GB.
180 The cells were carefully filled with GB and vibrated. The mass of GB porous medium inside the cells
181 was kept constant in order to ensure similar porous medium compaction and porosity characteristics.
182 The GB measured permeabilities were 1.30×10^{-10} m² and 6.73×10^{-12} m² for 0.5 mm GB and 0.1 mm
183 GB, respectively. At both extremities, the main cells were connected via two tubes to two graduated
184 “reservoir” columns (3.5 cm internal diameter and 41.8 cm high). These two reservoirs (containing
185 respectively water and DNAPL) stored the fluids and allowed to control the pressure heads at the
186 lower and upper parts of the cell. The cells and the columns were made of PolyVinylidene Fluoride
187 (PVDF) and were connected by thermo-scientific Nalgene 8001-1014 | 180 metric clear PolyVinyl
188 Chloride (PVC) tubes with 1 cm internal diameter. The volumes of DNAPL and water in the porous
189 media were calculated by volume balance. The addition of surfactants and the heating up to 50 °C
190 were carried out at the end of the drainage periods in order to start with the same values of S_{rw} as for
191 the experiments without enhancement. The experimental set-up was also constantly monitored by
192 geophysics and TDR probes. The number of drainage-imbibition experiments performed with 0.5 and
193 0.1 mm GB were respectively: 5 and 6 without enhancement and with membrane, 3 and 4 without
194 enhancement and without membrane, 8 and 6 with surfactants, 2 and 2 with thermal enhancement.

195 The curves, which were afterwards calibrated using the van Genuchten-Mualem model (VGM),
196 provide key parameters such as the irreducible water saturation (S_{rw}), the residual pollutant saturation
197 (S_m), the entry pressure, and the calibration parameters α and n which characterize the capillary forces
198 and the heterogeneity of the porous medium, respectively (Eq. 1 and Eq. 2) [Mualem (1976); van
199 Genuchten (1980)].

$$S_{ew} = \frac{1}{[1 + (\alpha h_c)^n]^m} \quad \text{Eq. 1}$$

$$S_{ew} = \frac{S_w - S_{rw}}{1 - S_{rw} - S_{rn}} \quad \text{Eq. 2}$$

200 where $m = 1-1/n$, $S_{ew} (-)$ is the effective water saturation, $h_c (m)$ is the capillary pressure head, $\alpha (m^{-1})$ is
 201 a fitting parameter that is inversely proportional to the non-wetting fluid entry pressure value, and $n (-)$
 202 is the width of pore-size distribution.

203 The experimental data were fitted to the VGM capillary pressure-saturation function using the
 204 solver provided in Excel by minimizing the Sum of Squared Errors (SSE).

205

206 2.4 Monitoring of the drainage-imbibition experiments with dielectric permittivity

207 Dielectric permittivities were monitored using TDR probes (Decagon Devices 5TE 40567) with a
 208 70 MHz frequency. Data acquisition frequency was 2 signals per minute. In addition to permittivity (-
 209), these probes monitor volumetric water content-VWC ($m^3.m^{-3}$), temperature ($^{\circ}C$), and bulk electrical
 210 conductivity-EC ($dS.m^{-1}$). They were connected to a Campbell Scientific CR1000 (4M) data logger to
 211 acquire temperature and permittivity data. The permittivity values were corrected relative to the
 212 reference values measured in air and water using the following equation (Eq. 3) [Kargas and Soulis
 213 (2012)]:

$$\varepsilon_{corrected} = \frac{\varepsilon_{w-theoretical}(\varepsilon_{measured} - \varepsilon_{air})}{(\varepsilon_w - \varepsilon_{air})} + \varepsilon_{air-theoretical} \quad \text{Eq. 3}$$

214 where $\varepsilon_{w-theoretical} (-)$ is the relative effective permittivity of pure water ($\varepsilon_{w-theoretical} = 80$ at $20^{\circ}C$),
 215 $\varepsilon_{measured} (-)$ is the relative effective permittivity of the medium measured with the TDR probe during the
 216 experiments, $\varepsilon_{air} (-)$ is the relative effective permittivity of air measured at the beginning of the
 217 experiment, $\varepsilon_w (-)$ is the relative effective permittivity of tap water measured at the beginning of the
 218 experiment, and $\varepsilon_{air-theoretical} (-)$ is the relative effective permittivity of pure air ($\varepsilon_{air-theoretical} = 1$).

219

220 2.5 Monitoring of the drainage-imbibition experiments with electrical resistivity

221 Electrical resistivity was monitored using unpolarizable potential electrodes for voltage
 222 measurement, metallic current electrodes for current injection, a resistivity meter and data acquisition

223 software. To limit electrode polarization phenomena, which can add noise to the measurements,
224 potential electrodes must be unpolarizable [Dahlin (2000)]. Cu/CuSO₄ electrodes were used and the
225 method developed by Noel [Noel (2014)]. These electrodes were made by mixing milli-Q water
226 72.2%, CuSO₄ 26% and Gelatin 1.7% and heated the mixture to ≈80 °C for 45 minutes using a
227 shaking heating plate. The resulting electrodes are unpolarizable, *i.e.*, they do not polarize the ground
228 and therefore the electrode action on the potential measured can be considered negligible.

229 The metallic current electrodes were made of nickel-cobalt alloy (MP35N). The resistivity meter
230 was SIP LAB IV and data acquisition software was SIP LAB IV. Resistivity was measured between
231 0.1 to 20 000 Hz but analysed at 1.4 Hz. This frequency was chosen because it is close to that used in
232 the field [Chambers et al. (2004); Constable and Srnka (2007); Han et al. (2015); Deparis et al.
233 (2019)]. The Wenner electrodes configuration was applied, as it well suited for cell experiments [Noel
234 (2014)].

235 The values measured were resistance values, R_e , which were transformed into apparent electrical
236 resistivity values, ρ_c , using the geometric coefficient, K_g (Eq. 4 and Eq. 5) [Reynolds (2011)] :

$$K_g = \frac{R_0}{R_e} \quad \text{Eq. 4}$$

$$\rho_c = R_e K_g \quad \text{Eq. 5}$$

237 where K_g (m) is the geometric coefficient, and R_0 ($\Omega \cdot m$) is the initial estimated resistance value.

238 The conductivity of the tap water, measured at the beginning of each experiment, made it possible
239 to determine R_0 and to calculate K_g (using Eq. 4). The value of K_g was then used throughout the
240 experiment to transform R_e into ρ_c .

241 Experiments were carried out to quantify the impact of chemical and thermal enhancements on
242 permittivities and resistivities: drainage experiments were first performed with only tap water and GB
243 by (i) introducing tap water with surfactants (at their CMC values) and (ii) increasing temperature.
244 Experiments were then performed in order to quantify the effects of temperature on the permittivity
245 and resistivity of DNAPL, water, DNAPL+GB, and water+GB systems. In these experiments,
246 temperature was increased stepwise from 10 to 50 °C. Permittivity and resistivity were noted once the

247 temperature of each step had stabilized. The correlation curves helped to correct the permittivity and
248 resistivity values with temperature variations.

249

250 2.6 *Monitoring of the drainage-imbibition experiments with image interpretation*

251 The optical imaging method used was the light reflection method (LRM), with a Nikon® D810
252 with NIKKOR LENS 105 (Nikon®) digital camera which has a high resolution of 34 Mega Pixels. The
253 image resolution calculated from Fiji (open source image processing package based on ImageJ) for these
254 experiments was approximately $0.003 \text{ mm}^2 \cdot \text{pixel}^{-1}$, depending on the image size [pixels×pixels] and the
255 distance between the camera and the object of interest. The following camera set up was used: aperture
256 = 1/200 s, ISO = 100 and the shutter = f/16. This set up remained the same during all experiments. The
257 Capture One® software was used to take photographs without touching the camera. All pictures were
258 acquired on RAW format (.raw) to save the full data information.

259 For the calibration, the drainage-imbibition experiments were conducted in the same way as with
260 1D cells but this time with a Hele-Shaw cell (to prevent light reflection). The dimensions of this cell
261 were: height = 5.00 cm, length = 5.00 cm and width = 2.00 cm. The cell was made of PVDF (as with
262 the 1D cells), to ensure high chemical resistance to the pure pollutant. The cell was composed of two
263 transparent glass faces to allow photographing. The experiments were performed in a dark room and
264 the light source was provided by two 2×300 W floodlights (Broncolor®). The camera was always
265 placed in the same position for all experiments. A color scale was placed beside the cell to calibrate
266 the differences, albeit small, between the lighting used for the various experiments.

267 First, a global Area Of Interest (AOI) was defined to obtain the mean grey value necessary to
268 associate with S_w . Then each picture was converted into 8-bit format. Finally, the mean grey values
269 were calculated using Fiji software, for different AOI centered in the middle of the picture. Fiji
270 software was chosen because it is easy to apply a threshold that depends on the pixel intensity value.
271 The threshold depends on the calibration curve fluid saturation versus intensity. Using Fiji, it is
272 possible to determine the area associated with the threshold. From this information (DNAPL saturation
273 and its own area), one can compute the DNAPL volumes present using the following expression (Eq.
274 6).

$$V_{DNAPL} = S_{DNAPL} A_{DNAPL} l \emptyset \quad \text{Eq. 6}$$

275 where V_{DNAPL} (m³) is the volume of DNAPL for a given saturation, S_{DNAPL} (-) is the DNAPL
 276 saturation for a given threshold on Fiji, A_{DNAPL} (m²) is the area associated of the given saturation, l (m)
 277 is the length between the front wall and the back wall of the cell, and \emptyset (-) is the porosity.

278 The image data analysis was performed according to the following main steps: a) convert the
 279 picture into 8 bit format to obtain 256 shades of gray; b) set up the scale; c) set up the I_0 (Initial
 280 luminous intensity), which was equal to white on the gray scale; d) define the AOI; e) set up the
 281 contrast to optimize the black pixels; f) compute the layers of DNAPL saturation present on the AOI,
 282 based on the linear relation derived from the calibration experiment.

283

284 3. Theory

285 The parameters presented in section 2 provide information regarding the potential for mobilizing
 286 DNAPL in a porous medium, using various relationships or models. For example, Pennell *et al.* (1996)
 287 used a method to estimate DNAPL mobilization in the porous medium with capillary number (N_{ca}),
 288 Bond number (N_B) and total trapping number (N_T) (Eq. 7 to Eq. 9).

$$N_{ca} = \frac{v_w \mu_w}{\sigma \cos \theta} \quad \text{Eq. 7}$$

$$N_B = \frac{g k k_{rw} \Delta \rho}{\sigma \cos \theta} \quad \text{Eq. 8}$$

$$N_T = \sqrt{N_{ca}^2 + 2 N_{ca} N_B \sin \alpha_{N_T} + N_B^2} \quad \text{Eq. 9}$$

289 where v_w (m.s⁻¹) is the Darcy velocity of the wetting phase (upward direction is considered positive), μ_w
 290 (Pa.s) is the dynamic viscosity of the wetting phase, $\Delta \rho$ (kg.m⁻³) is the difference of densities between
 291 the wetting and non-wetting phase (= $\rho_w - \rho_n$), and α_{N_T} (°) is the angle between the direction of flow
 292 and the horizontal direction.

293 The mobility ratio (m_r) can be calculated as follows (Eq. 10) [Lenormand *et al.* (1988); Dullien
 294 (1992)]:

$$m_r = \frac{k_{2r} \mu_1}{k_{1r} \mu_2} \quad \text{Eq. 10}$$

295 where m_r (-) is the mobility ratio, k_{1r} (-) is the relative permeability for the displaced phase, k_{2r} (-) is
 296 the relative permeability for the displacing phase, μ_1 (Pa.s) is the fluid dynamic viscosity for the
 297 displaced phase, and μ_2 (Pa.s) is the fluid dynamic viscosity for the displacing phase.

298 Regarding the monitoring of permittivities to characterize saturations, the CRIM model has been
 299 developed for multiphase systems (Eq. 11) [Birchak et al. (1974); Roth et al. (1990); Endres and
 300 Knight (1992)]:

$$\varepsilon = \left[\sum_{i=1}^N v_i \varepsilon_i^{\alpha_\varepsilon} \right]^{1/\alpha_\varepsilon} \quad \text{Eq. 11}$$

301 where ε (-) is the relative effective permittivity of the mixture, ε_i (-) is the relative effective
 302 permittivity of the i phase, v_i (-) is the volume of the i phase, and α_ε (-) is an empirical constant
 303 related to the geometry of the grains and their spatial distribution.

304 Ajo-Franklin *et al.* (2004) report correlations higher than 97% using the CRIM model with TCE in
 305 the saturated zone [Ajo-Franklin et al. (2004)]. For a three-phase mineral/water/NAPL mixture and
 306 assuming that $\alpha_\varepsilon = 0.5$, the CRIM equation becomes (Eq. 12):

$$\varepsilon = \left[\phi (S_w \sqrt{\varepsilon_w} + S_n \sqrt{\varepsilon_n}) + (1 - \phi) \sqrt{\varepsilon_s} \right]^2 \quad \text{Eq. 12}$$

307 where S_w (-) is the water (wetting fluid) saturation, ε_w (-) is the relative effective permittivity of water,
 308 S_n (-) is the DNAPL (non-wetting fluid) saturation, ε_n (-) is the relative effective permittivity of
 309 NAPL, and ε_s (-) is the relative effective permittivity of soil particles.

310 For electrical resistivity interpretation, Archie's Law is described as follows (Eq. 13) [Archie
 311 (1942)]:

$$\rho_c = \rho_{c,w} a_c \phi^{-m_c} \quad \text{Eq. 13}$$

312 where ρ_c ($\Omega.m$) is the real effective electrical resistivity of the bulk, $\rho_{c,w}$ ($\Omega.m$) is the real effective
 313 electrical resistivity of the fluid at temperature T , a_c (-) is an empirical parameter (typically equal to 1
 314 but that can vary from <1 for intergranular porosity to > 1 for joint porosity), and m_c (-) is the
 315 cementing factor (also an empirical parameter usually approximately equal to 2, but that can vary from
 316 1.2 for unconsolidated sediments to 3.5 for crystalline rocks).

317 Glover (2010) proposed, on the basis of Archie's law, the following equations to calculate S_w for a two-
 318 phase system, where neglecting the conductivity of GB is neglected as it is very low ($\sigma_{c,GB} = 10^{-20} \text{ S.m}^{-1}$)
 319 (Eq. 14 to Eq. 17) [Glover (2010)]:

$$\sigma_{c,bulk} = \sigma_{c,DNAPL}[\phi(1 - S_w)]^{m_1} + \sigma_{c,water}[\phi(S_w)]^{m_2} \quad \text{Eq. 14}$$

$$\left(-\frac{\phi_1^2}{2}\right)m_2^2 + \left(\phi_1 + \frac{\phi_1^2}{2}\right)m_2 - \phi_1^{m_1} = 0 \quad \text{Eq. 15}$$

$$m_2 = \frac{-\left(\phi_1 + \frac{\phi_1^2}{2}\right) \pm \left[\left(\phi_1 + \frac{\phi_1^2}{2}\right)^2 - 4\left(-\frac{\phi_1^2}{2}\right)(-\phi_1^{m_1})\right]^{\frac{1}{2}}}{-\phi_1^2} \quad \text{Eq. 16}$$

$$m_2 = \frac{-(4\phi_1 + 2\phi_1^2) \pm (4\phi_1^2 + 4\phi_1^3 + \phi_1^4 - 8\phi_1^2\phi_1^{m_1})^{\frac{1}{2}}}{-4\phi_1^2} \quad \text{Eq. 17}$$

320 where $\sigma_{c,bulk} = \sigma_c \text{ (S.m}^{-1}\text{)}$ is the real effective electrical conductivity of the bulk, $\sigma_{c,DNAPL} \text{ (S.m}^{-1}\text{)}$ is
 321 the real effective electrical conductivity of DNAPL, $m_1 \text{ (-)}$ is the cementation exponent of DNAPL
 322 phase, $\sigma_{c,water} \text{ (S.m}^{-1}\text{)}$ is the real effective electrical conductivity of water, $m_2 \text{ (-)}$ is the cementation
 323 exponent of water phase, and $\phi_1 = \phi(1 - S_w)$; $\phi_2 = \phi(S_w)$.

324 For image analysis, the optical density of reflected light, D_r , can be defined as (Eq. 18 and Eq. 19)
 325 [Stimson (1974); Schincariol et al. (1993); Flores et al. (2011)]:

$$D_r = -\lg(\rho_t) \quad \text{Eq. 18}$$

$$\rho_t = \frac{I_r}{I_0} \quad \text{Eq. 19}$$

326 where: $D_r = \text{OD (-)}$ is the optical density of reflected light, $\rho_t \text{ (-)}$ is the ratio of reflected/initial
 327 luminous intensity, $I_r \text{ (-)}$ is the reflected luminous intensity, and $I_0 \text{ (-)}$ is the initial luminous intensity.

328

329 4. Results and discussion

330 4.1 Fluids characterization

331 4.1.1 Dynamic viscosity

332 While chlorinated solvents are typically more fluid than water (with viscosities less than 1 mPa.s)
 333 [Sleep and Ma (1997)], the dynamic viscosity of the DNAPL studied herein was much higher (5 mPa.s

334 at groundwater temperature, *i.e.* 12 °C). The viscosity of a chlorinated solvent is generally reduced by
335 1% per degree Celsius [Davis (1997)]. The dynamic viscosity of the DNAPL studied here reduced by
336 57% when the temperature rose from 10 to 60 °C, which is in agreement with the literature
337 (Supplementary materials, Figure A-1). As shown in this figure, the change in dynamic viscosity as a
338 function of temperature fitted a second order polynomial curve. For water, the reduction in dynamic
339 viscosity was 54% for the same temperatures. The μ_w/μ_{nw} ratio ranged from 0.23 to 0.19 for
340 temperatures of 10 °C and 60 °C, respectively. This 15% reduction in viscosity ratios may contribute
341 to improve DNAPL mobility.

342

343 4.1.2 *Interfacial tension and contact angle between DNAPL and water*

344 The IFT, σ , was measured as 11.15 ± 0.05 mN.m⁻¹ at 20°C (Supplementary materials, Figure A-2).
345 This value was lower than that of pure TCE or PCE in distilled water (respectively 36.9 and 45.9
346 mN.m⁻¹) [Andersson et al. (2014)]. The results for reduced interfacial tensions with added surfactants
347 were very contrasted. Three trends were observed: a moderate effect for Tween 80, a substantial effect
348 for relatively high CMC of Triton X-100 and Aerosol MA-80, and a very substantial beneficial effect
349 for low surfactant concentrations of SDBS. More precisely, we found that the reduction in IFT for
350 Tween 80 was 52% with the concentration of 64×CMC ($\sigma_{\text{final}} = 5.28$ mN.m⁻¹). As for Triton X-100 and
351 Aerosol MA-80, the reductions were respectively 96% and 90% for a concentration of 64×CMC (σ_{final}
352 = 0.48 mN.m⁻¹ and 1.10 mN.m⁻¹). Finally, SDBS seemed to be the most advantageous surfactant as it
353 could reduce the IFT by 99% at a lower surfactant concentration ($\sigma_{\text{final}} = 0.10$ mN.m⁻¹). Experimental
354 results showed that thermal enhancement had only limited influence on DNAPL/water IFT. This
355 parameter decreased by only 2.3% between 10 and 60 °C (respectively 12.17 to 11.89 mN.m⁻¹).

356 The DNAPL-water-glass contact angle without surfactant was 119.33 ± 4.16 ° at 20 °C
357 (Supplementary materials, Figure A-3), which is typical of such a non-wetting fluid and close in order
358 of magnitude to values reported in the literature (*e.g.*, 129° for TCE in pure water) [Orphius and
359 Kibbey (2005)]. The reduction in contact angles with chemical enhancement were consistent with
360 previous work [Amirpour et al. (2015)]. The contact angle was significantly reduced by adding SDBS;
361 it reached 30.33° (*i.e.* a 75% drop) for SDBS concentrations far below the CMC and therefore DNAPL

362 became wetting, as the angle was less than 90°. Regarding the other anionic surfactant, adding Aerosol
363 MA-80 reduced the contact angle by 23% for a concentration equivalent to 16×CMC ($\theta_{\text{final}} = 91.33^\circ$).
364 The two nonionic surfactants gave similar curves. Triton X-100 and Tween 80 only reduced the
365 contact angles by 5.6 and 4.9% ($\theta_{\text{final}} = 112.70^\circ$ and 113.50°), respectively. The temperature increase
366 only moderately reduced the contact angle. Increasing the temperature from 10 to 60 °C decreased the
367 contact angle from 126.33 to 108.00° (*i.e.* a 14% reduction).

368 Based on these results, we can estimate the effect of chemical and thermal enhancements on
369 capillary pressure, P_c . As a first approximation, we considered DNAPL and water in a tube (pore
370 throat) with a circular cross section (Eq. 20).

$$P_c = \frac{2\sigma\cos\theta}{r} \quad \text{Eq. 20}$$

371 where P_c (Pa) is the capillary pressure, $\sigma = \sigma_{\text{nw}}$ (mN.m⁻¹) is the interfacial tension, θ (°) is the pore
372 contact angle, and r (cm) is the mean radius of interface ($r = r_{\text{tube}}/\cos\theta$)

373 The nonionic surfactants reduced P_c less than the anionic surfactants. Triton X-100 and Tween 80
374 only reduced the capillary pressure by 77.3% and 62.5%, respectively, while the anionic surfactants
375 were far more effective in reducing capillary pressure (respectively, 98.9% and 99.7% for Aerosol
376 MA-80 and SDBS). Thermal enhancement had only a minor effect on P_c (49.4% reduction).

377

378 4.1.3 Density

379 The studied DNAPL was denser (1.66 kg.L⁻¹ at 20 °C) than well-known chlorinated solvents such
380 as TCE and PCE (respective densities at 20 °C: 1.46 and 1.62 kg.L⁻¹). PCE density variations as a
381 function of temperature are moderate; with decreases on the order of 0.1 kg.L⁻¹ for a temperature
382 increase from 20 to 90 °C [Sleep and Ma (1997)]. The Tavaux site DNAPL also displayed a moderate
383 density decrease as a function of temperature; as the density decreased only by 3% for temperatures
384 ranging from 10 to 60 °C (Supplementary materials, Figure A-4).

385

386 4.2 Solubilization

387 The DNAPL solubility was low: 40.00 mg.L^{-1} (at $20 \text{ }^\circ\text{C}$) (Supplementary materials, Figure A-5).
388 The two non-ionic surfactants generated a global solubility increase ($\Sigma[\text{COC}]$) of a factor of 20 for
389 Triton X-100 (for a concentration of $8 \times \text{CMC}_{\text{theoretical}}$) whereas it was only 1.45 for Tween 80 for the
390 same concentration ratio. The addition of MA-80 aerosol at $8 \times \text{CMC}$ increased the solubilization
391 yielded by a factor of 18; but only by a factor of 1.3 for SDBS with the same CMC ratios. Usually, as
392 surfactant concentration increases, the volume of core micelles increases, leading to a linear increase
393 in the apparent solubility [Pennell et al. (2014)]. A linear change in apparent solubility has also been
394 demonstrated for surfactant concentrations greater than their CMC for several chlorinated compounds
395 (*e.g.*, PCE, TCE, HCBd and HCEa) [Jafvert (1994); Kommalapati et al. (1997); Harendra and
396 Vipulanandan (2011); Rodrigues et al. (2017)].

397 The CMC_{real} of the surfactants that correspond to the $\text{IFT} = f([\text{surfactant}])$ and $[\Sigma\text{COC}] =$
398 $f([\text{surfactants}])$ curves' inflection points are (Supplementary materials, Figure A-5): $1200.00 \text{ mg.L}^{-1}$
399 for Triton X-100, 503.04 mg.L^{-1} for Tween 80, $11640.00 \text{ mg.L}^{-1}$ for Aerosol MA-80 and 65.34 mg.L^{-1}
400 for SDBS. Increasing the temperature from $12 \text{ }^\circ\text{C}$ (temperature of the groundwater) to $60 \text{ }^\circ\text{C}$ increased
401 the solubility by 13% (44.16 versus 50.00 mg.L^{-1}), which is relatively small change.

402

403 4.3 Drainage-imbibition experiments

404 4.3.1 Drainage-imbibition experiments without enhancement

405 The P_c - S_w curves for 0.5 and 0.1 mm GB are compared in Figure 2a. Table 1 shows the results of
406 these experiments and the van Genuchten-Mualem (VGM) fitting parameters. The experimental data
407 were fit to the VGM capillary pressure-saturation function (Eq. 1 and Eq. 2) using sum of squared
408 errors (SSE) minimization. The SSE were low ($\text{SSE} < 0.0014$), which demonstrated that the VGM
409 model can be used to describe the experimental results. The experimental results are mainly focused
410 on residual DNAPL saturation and irreducible water saturation. It is clear from the graph that the
411 parameters differed slightly for each size of glass bead. For 0.5 mm GB, S_{rn} was approximately 10.9%
412 vs. 12.7% for 0.1 mm GB. According to the results, S_{rw} was around 24.8% for 0.5 mm GB and 30.9%
413 for 0.1 mm GB. This is explained by capillary forces as the mean pore radius was higher for 0.5 mm

414 GB and therefore the influence of capillary forces was lower. Therefore, during drainage, less DNAPL
 415 could be incorporated into the 0.5 mm GB medium (S_{rn} was 23.0% higher than for 0.1 mm GB) while
 416 during imbibition, more DNAPL trapped in the 0.5 mm GB medium could be extracted (S_{rn} was
 417 16.0% higher than for 0.1 mm GB). The curve for 0.1 mm GB has a lower S_w amplitude. These results
 418 are in agreement with the data reported in the literature [Mualem (1976); van Genuchten (1980);
 419 Gerhard and Kueper (2003a)].

420 The parameter α value, characteristic of the reverse of the suction effects, was higher for the 0.5
 421 mm GB, which was expected, since capillary effects were higher for the 0.1 mm GB. The slope of the
 422 median portion of the curves was relatively flat, which confirms that the GB were indeed
 423 homogeneous [Ouchiyama and Tanaka (1984); Likos and Jaafar (2013); Chapuis et al. (2015);
 424 Chiapponi (2017)]. The interpretation of parameter n values variations is more complex: sensitivity
 425 tests show that for high α values and n values greater than 4 (in a homogeneous medium), as in our
 426 case, the variations of n had a minor influence on the shape of the retention curves.

427

428 4.3.2 Drainage-imbibition experiments with enhancements

429 The remediation enhancement yield was calculated as follows (Eq. 21):

$$430 \text{ Remediation yield} = 100 - 100 \left(\frac{S_{rn, \text{chemical enhancement}}}{S_{rn, \text{without enhancement}}} \right) \quad \text{Eq. 21}$$

431 Adding SDBS had the highest impact on reducing the IFT. Therefore, the best remediation
 432 enhancement yield was obtained with SDBS (27.6% *i.e.* $S_{rn} = 0.079$), for 0.5 mm GB. Aerosol MA-80
 433 and Triton X-100 had similar remediation enhancement yields (24.0 and 22.5% respectively, *i.e.* $S_{rn} =$
 434 0.083 and 0.085). Tween 80 had a remediation enhancement yield close to zero ($S_{rn} = 0.11$). For 0.1
 435 mm GB, the best remediation enhancement yield was with SDBS (46.3% *i.e.* $S_{rn} = 0.068$). Aerosol
 436 MA-80 performed better than Triton X-100: the remediation enhancement yields were respectively
 437 35.56 and 38.1% ($S_{rn} = 0.082$ and 0.078). Tween 80 had a remediation enhancement yield of 7.0% (S_{rn}
 438 = 0.118).

439 The remediation enhancement yields for 0.1 mm GB were higher than those observed with the 0.5
 mm GB. This is because the capillary forces were higher for 0.1 mm GB and the effect of the

440 surfactants, whose purpose is to reduce the IFT, is improved. The best results were obtained with
441 SDBS. Figure 2b shows the average of the experimental results for P_c - S_w curves with SDBS
442 (imbibition) for the 0.5 mm GB and 0.1 mm GB (fitted with the VGM model). At the end of drainage,
443 adding surfactant influences the slope of the line, which is slightly more horizontal, demonstrating that
444 the capillary effects, and therefore the capillary fringes (thickness of the migration front), were weaker.

445 Capillary number (N_{ca}), Bond number (N_B), and Total trapping number (N_T) were calculated using
446 Eq. 7 to Eq. 9 on the basis of the experimental and rheological data (Figure 3). As expected, increasing
447 the grain size increases all three numbers. Here, viscosity forces predominate over gravitational forces,
448 while capillary forces predominated over other forces. Adding surfactants increased N_{ca} and
449 consequently N_T . Increasing N_{ca} decreases the residual saturations [Lake (1989); Pennell et al. (1996);
450 Sheng (2015)]. It was found that the thermal enhancement had no effect on S_m or on the shape of the P_c -
451 S_w curve during the imbibition stage of these static drainage-imbibition experiments. The thermal
452 enhancement only affected the viscosity.

453

454 4.4 *Monitoring of the drainage-imbibition experiments with dielectric permittivity*

455 4.4.1 *Drainage-imbibition experiments without enhancement*

456 Permittivity calibration curves were plotted as a function of water saturation for 0.5 and 0.1 mm
457 GB (Figure 4). Permittivity could be related to water saturation by a second order polynomial
458 relationship. The scatter plot was less dispersed for the 0.5 mm GB than for the 0.1 mm GB and
459 therefore R^2 was lower for the 0.1 mm GB ($R^2 = 0.79$ vs 0.90 for 0.5 mm GB). This can be explained
460 by the difference between capillary effects.

461 The resulting trends were very similar for 0.5 and for 0.1 mm GB. The calibration curves were also
462 very similar: the ratios of polynomial curves for 0.5 mm GB/polynomial curves for 0.1 mm GB vary
463 between 0.97 and 1.20. For homogeneous porous media, grain size has little influence on permittivity.
464 These results were consistent with previous research on permittivities measured in a water-air system.
465 The small differences can be attributed to the less regular GB, the spherical shape of GB and the pore
466 connectivity [Robinson and Friedman (2001); Robinson and Friedman (2002); Robinson et al. (2005);
467 Brovelli and Cassiani (2010)].

468 Experimental data was fitted to the CRIM model (see Eq. 12), using the following values: $\emptyset = 0.38$
 469 (experimental values), $\varepsilon_w = 80$ (experimental value), $\varepsilon_n = 3.11$ (experimental value for 100% DNAPL),
 470 $\varepsilon_m = 7.5$ (literature review for GB material [von Hippel (1954); Robinson and Friedman (2002)]).

471 We see that a value $\alpha_e = 0.5$ (cited in the literature) does not fit our experiments. The α_e values
 472 calculated by the least-square method were respectively 0.70 and 0.75 for 0.5 mm and 0.1 mm GB
 473 (with respective R^2 of 0.89 and 0.78). Therefore, for our experiments the CRIM model can be applied
 474 using the following equations (Eq. 22 to Eq. 23):

$$\text{For 0.5 mm GB} \quad \varepsilon' = [\emptyset(S_w \varepsilon_w'^{0.7} + S_n \varepsilon_n'^{0.7}) + (1 - \emptyset) \varepsilon_m'^{0.7}]^{\frac{1}{0.7}} \quad \text{Eq. 22}$$

$$\text{For 0.1 mm GB} \quad \varepsilon' = [\emptyset(S_w \varepsilon_w'^{0.75} + S_n \varepsilon_n'^{0.75}) + (1 - \emptyset) \varepsilon_m'^{0.75}]^{\frac{1}{0.75}} \quad \text{Eq. 23}$$

475 Figure 4 shows a satisfactory match between the experimental data and the CRIM model for higher
 476 saturations than S_{rw} (less than 8% difference). The CRIM model fitted the data better for 0.5 mm GB.
 477 For lower water saturation, the ratios between the values estimated and the experimental values
 478 increased. The estimated values were overestimated by a factor of 1.14 for 0.5 mm GB and were
 479 underestimated by a factor of 0.92 for 0.1 mm GB. Persson and Berndtsson (2002) also obtained a
 480 better match to their data by introducing an extra degree of freedom in the mixing equations [Persson
 481 and Berndtsson (2002)].

482 Figure 5 illustrates permittivity variations as a function of different drainage-imbibition cycles. The
 483 drainage-imbibition experiments could be closely correlated with permittivities but after the end of the
 484 second cycle (end of imbibition 2), the correlation no longer held. This is probably because the
 485 DNAPL and water ganglions that remain trapped during the experiments influenced the dielectric
 486 response.

487 Some authors have shown that the CRIM model based on the relative permittivity of free water, air
 488 (or non-wetting fluid) and solids may not be suitable in all situations, especially in the transition
 489 phases (when S_w are between S_m and S_{rw}). These authors have proposed to consider a 4th constituent,
 490 the bound water. Indeed, the dielectric constant of bound water is very different from that of free water
 491 (due to the electrical bonds limiting the freedom of polarization of water molecules) [Dasberg and
 492 Hopmans (1992); Capparelli et al. (2018)]. An equation derived from the CRIM model incorporating

493 the bound water has been proposed [Dobson et al. (1985); Dirksen and Dasberg (1993)]. Capparelli et
494 al. (2018) carried out monitoring of S_w variations with TDR probes in unsaturated soils. They showed,
495 as in our experimental results, a difference between the values estimated with the CRIM model and the
496 experimental values. The experimental results were compared to the classical CRIM model, to the
497 four-phase dielectric mixing model (with bound water), and to the classical CRIM model with a
498 variable exponent. The best results were obtained with the three-phase dielectric mixing model with a
499 variable exponent (α_ϵ) [Capparelli et al. (2018)].

500

501 4.4.2 *Drainage-imbibition experiments with enhancements*

502 Relative to the response considered as the blank test (water + GB), the mean measured
503 permittivities were impacted by +1.4% (SDBS), +0.5% (Aerosol MA-80), -1.6% (Triton X-100), and -
504 2.1% (Tween 80), respectively. It was observed, therefore, that the permittivity was slightly increased
505 for nonionic surfactants and slightly decreased for anionic surfactants. But such deviations can be
506 considered as negligible. Figure 5 shows the averages of S_m with permittivity averages corresponding
507 to the experiments with and without surfactants (with 0.1 and 0.5 mm GB). Even though the standard
508 deviations sometimes overlap, we can assess the recovery yields from the permittivity measurements:
509 the average permittivities for 0.5 and 0.1 mm GB without surfactants were respectively 27.77 and
510 25.32 (for S_w at the end of imbibition = 0.89 and 0.87). In presence of surfactants, the average
511 permittivities for 0.5 mm GB and 0.1 mm GB were respectively 29.07 and 30.81 (for S_w at the end of
512 imbibition of 0.915 and 0.917). Figure 5 also shows the permittivity variations that correspond to the
513 different remediation yields (for different surfactants): for the 0.5 mm GB, the final permittivities are,
514 in increasing order: $\rho_{c,SDBS} > \rho_{c,Aerosol\ MA-80} > \rho_{c,Triton\ X-100} > \rho_{c,Tween\ 80}$. The averages overestimations for
515 S_m with chemical enhancement were by a factor of 1.06 ± 0.02 (for 0.5 mm GB) and 1.09 ± 0.01 (for
516 0.1 mm GB).

517 Experiments were conducted to estimate the influence of temperature on measured permittivities
518 for DNAPL and water with 0.5 mm GB (Supplementary materials, Figure A-6). The permittivity
519 values were influenced by temperature variations. Increasing the temperature from 20 to 50 °C caused
520 an average permittivity increase for DNAPL with GB of 19.0% (from 5.45 to 6.49). The variation in

521 $\epsilon_{\text{DNAPL+GB}}$ as a function of temperature, estimated from the slopes of the linear correlations, is + 0.034
522 $\text{m}^3\cdot\text{m}^{-3}\cdot^{\circ}\text{C}^{-1}$. Results from various authors show that the permittivity of light chlorinated solvents fall
523 slightly as temperature rises. A linear relation has been established, with coefficients ranging between
524 -0.003 and -0.051 $\text{m}^3\cdot\text{m}^{-3}\cdot^{\circ}\text{C}^{-1}$ [Morgan and Lowry (1930); Loon et al. (1967); Nath and Narain
525 (1982); Nath (1995); Corradini et al. (1996); Ajo-Franklin et al. (2006)]. In our case, the DNAPL is
526 essentially composed of a mixture of heavy chlorinated compounds, which may explain the difference
527 in behavior.

528 Permittivities for water with GB decreased linearly as temperature rose ($0.023 \text{ m}^3\cdot\text{m}^{-3}\cdot^{\circ}\text{C}^{-1}$), with
529 values that were consistent with the literature [Weast (1986); Persson and Berndtsson (1998); Logsdon
530 (2000); Logsdon (2005); Seyfried and Grant (2007)]. The variations in $\epsilon_{\text{DNAPL+GB}}$ and $\epsilon_{\text{water+GB}}$ as a
531 function of temperature were quantified and can be interpreted with the CRIM model. At the end of
532 imbibition, the measured permittivities were 28.50 and 25.58 for 0.5 and 0.1 mm GB, respectively (vs
533 estimated permittivities of 26.89 and 27.12, respectively). The experiments with surfactants and
534 thermal enhancement showed that the reductions in residual saturations can be quantified with
535 permittivity measurements.

536

537 4.5 *Monitoring of the drainage-imbibition experiments with electrical resistivity*

538 4.5.1 *Drainage-imbibition experiments without enhancement*

539 Calibration curves ($\rho_c = f(S_w)$) were plotted for 0.5 and 0.1 mm GB (Figure 6). Experiments with
540 DNAPL alone in GB were performed to determine the experimental values corresponding to $S_w = 0\%$
541 and $S_w = 100\%$. Resistivity data were found to be more dispersed than permittivity data. Resistivity
542 can be correlated to water saturation via a power relationship. The correlation factor, considering all
543 the measured data, was satisfactory for 0.5 mm GB: $R^2 = 0.81$. The results were more dispersed with
544 the 0.1 mm GB than with the 0.5 mm GB. Resistivity was related to S_w via a power law for 0.1 mm
545 GB; with a correlation factor $R^2 = 0.74$. The results were different for 0.5 and 0.1 mm GB: the features
546 of the trend curves are similar but are shifted. For homogeneous beads, and for identical S_w , the
547 resistivity was higher for the 0.1 mm GB. This can be explained by the difference in DNAPL
548 distributions in pores.

549 On the basis of Eq. 14 to Eq. 17 and by applying the least-squares method, we obtained the
 550 following equations (Eq. 24 and Eq. 25):

$$\text{for 0.5 mm GB} \quad \rho_{c,bulk} = \frac{1}{\sigma_{c,bulk}} = \frac{1}{\sigma_{c,DNAPL}[\emptyset(1 - S_w)]^{1.752} + \sigma_{c,water}[\emptyset(S_w)]^{1.9}} \quad \text{Eq. 24}$$

$$\text{for 0.1 mm GB} \quad \rho_{c,bulk} = \frac{1}{\sigma_{c,bulk}} = \frac{1}{\sigma_{c,DNAPL}[\emptyset(1 - S_w)]^{1.678} + \sigma_{c,water}[\emptyset(S_w)]^{2.4}} \quad \text{Eq. 25}$$

551 where $\rho_{c,bulk}$ ($\Omega.m$) is the real effective electrical resistivity of the bulk, and $\rho_{c,DNAPL}$ ($\Omega.m$) is the
 552 real effective electrical resistivity of DNAPL.

553 The conductivity values measured for DNAPL and water used to fit the model were: $\sigma_{c,DNAPL} = 3.1807 \times 10^{-8}$
 554 $S.m^{-1}$ and $\sigma_{c,water} = 0.04 S.m^{-1}$.

555 A correction factor was used in order to better estimate the experimental data. The correction
 556 factors were as follows (Eq. 26 and Eq. 27):

$$\text{for 0.5 mm GB} \quad \frac{\rho_{c,measured}}{\rho_{c,estimated}} = 1.34S_w^{0.40} \quad \text{Eq. 26}$$

$$\text{for 0.1 mm GB} \quad \frac{\rho_{c,measured}}{\rho_{c,estimated}} = 2.00S_w - 0.011 \quad \text{Eq. 27}$$

557 Figure 7 illustrates the resistivity variations (measured and estimated) as a function of different
 558 drainage-imbibition cycles. The model overestimated the values at the start and under-estimated the
 559 values in most other cases. For the 0.5 mm GB, the average ratios of measured resistivity/estimated
 560 resistivity were 0.64 for $S_w = 100\%$ (start), 3.14 at the end of the drainage 1 and 0.99 at the end of the
 561 imbibition 1. For the 0.1 mm GB, these ratios were 0.72 at the start, 12.84 at the end of drainage 1 and
 562 5.22 at the end of imbibition 1. As for permittivity, it reminded that the resistivity measurement is very
 563 local while the water saturation measurement is more global. Uncertainty is higher for large resistivity
 564 values because the measured potential difference is smaller.

565 These resistivity overestimations have been discussed by previous authors. Byun et al. (2019)
 566 showed that in a porous medium with water and gas, a cementation factor that considers the saturation
 567 condition improves resistivity modeling with Archie's law [Byun et al. (2019)]. Other authors also
 568 demonstrated that at pore scale, the resistivity indices did not generally obey Archie's law in the non-
 569 homogeneous zones (for example in a transition zone with values close to S_{rn} and S_{rw}). It is therefore

570 possible to over or underestimate resistivity depending on the thickness of the water films surrounding
571 sand grains or GB [Li et al. (2015)]. These water films play a role not only on the pore space
572 connectivity but also on resistivity [Bernabé et al. (2011); Li et al. (2015); Bernabé et al. (2016)].
573 Finally, previous authors have shown that many other parameters could be taken into account at
574 different scales in electrical conductivity models in porous media: tortuosity, pore size distribution,
575 pore-conductance distributions, interconnectivity, and universal power laws of percolation [Glover
576 (2010); Cai et al. (2017); Ghanbarian and Sahimi (2017)].

577

578

579

580 4.5.2 *Drainage-imbibition experiments with enhancements*

581 The experimental results show that adding surfactants generated a greater impact on resistivity
582 measurements than on permittivity measurements. For mean reference values of $132 \pm 17 \text{ } \Omega \cdot \text{m}$ (for
583 water+GB), the mean values measured for nonionic surfactants were respectively $123 \pm 21 \text{ } \Omega \cdot \text{m}$ for
584 SDBS and $30 \pm 9 \text{ } \Omega \cdot \text{m}$ for Aerosol MA-80 (*i.e.* a factor of 0.92 and 0.22). Conversely, adding anionic
585 surfactants increased resistivity: $216 \pm 25 \text{ } \Omega \cdot \text{m}$ for Triton X-100 and $140 \pm 19 \text{ } \Omega \cdot \text{m}$ for Tween 80, *i.e.*
586 respective increased of a factor of 1.62 and 1.05. However, these relative variations were small in
587 comparison with the resistivity of the DNAPL and GB ($\rho_{c, \text{DNAPL}} = 2730063$ and $3413632 \text{ } \Omega \cdot \text{m}$
588 respectively for 0.5 and 0.1 mm GB) and considering the high sensitivity and low accuracy of these
589 geophysical measurements at very low frequencies. Such variations can therefore be considered as
590 negligible.

591 Figure 7 shows the averages of S_{m} with averaged resistivity corresponding to the experiments with
592 and without surfactants (with the 0.1 and 0.5 mm GB). As shown, the residual saturations can be
593 approached by the resistivity measurements. The correlations were less clear with resistivities than
594 with permittivities. Decreasing trends for S_{m} are seen in the resistivity measurements. For the 0.5 mm
595 GB, for example, the resistivities at the end of the imbibition with and without surfactant were
596 respectively 150 and 84 $\Omega \cdot \text{m}$ (for S_{m} of 0.109 and 0.085). For 0.1 mm GB, the differences were

597 greater: 1061 $\Omega\cdot\text{m}$ (without surfactants with $S_{\text{rn}} = 0.131$) vs. 79 $\Omega\cdot\text{m}$ (with surfactant with $S_{\text{rn}} = 0.082$).
 598 The reported standard deviations were quite high for imbibition without surfactant.

599 Experiments were conducted to estimate the influence of temperature on measured resistivities of
 600 water and DNAPL. The resistivity of DNAPL at 50 $^{\circ}\text{C}$ only represented 25.3% of the resistivity at 20
 601 $^{\circ}\text{C}$ (5.88×10^5 vs. 2.32×10^6 $\Omega\cdot\text{m}$, respectively at 50 and 20 $^{\circ}\text{C}$). The resistivity values of water were
 602 very low compared to those of DNAPL. Resistivity values were 31 $\Omega\cdot\text{m}$ at 20 $^{\circ}\text{C}$, and 17 $\Omega\cdot\text{m}$ at 20 $^{\circ}\text{C}$
 603 (*i.e.* 57% of the value at 20 $^{\circ}\text{C}$). The decrease in water resistivity as a function of temperature increase
 604 was due to the increase in ionic mobility [Dakhnov (1962); Hayashi (2004); Light et al. (2005);
 605 Grellier et al. (2008)]. Dakhnov (1962) established the following relationship (for ionic fluids) (Eq.
 606 28):

$$\rho_{c,w} = \frac{\rho_{c,w_0}}{1 + \alpha_{c,w}(T - T_0)} \quad \text{Eq. 28}$$

607 where $\rho_{c,w}$ ($\Omega\cdot\text{m}$) is the electrical resistivity of the fluid at temperature T ($^{\circ}\text{C}$), ρ_{c,w_0} ($\Omega\cdot\text{m}$) is the
 608 resistivity of the fluid at temperature T_0 , $\alpha_{c,w}$ is the temperature coefficient of resistivity ($\alpha_{c,w} \approx 0.023$
 609 $^{\circ}\text{C}^{-1}$ for $T_0 = 23$ $^{\circ}\text{C}$, and 0.025 $^{\circ}\text{C}^{-1}$ for $T_0 = 0$ $^{\circ}\text{C}$)

610 The slopes of the linear relationships in the graphs $(\rho_{c,0}/\rho_c) - 1 = f(T - T_0)$ determine the values of the
 611 coefficient α_c for the Dakhnov equation (Supplementary materials, Figure A-7).

612 With respect to the drainage-imbibition experiments with thermal enhancement, the residual
 613 saturations were almost identical with and without thermal enhancement. $\rho_{c,\text{measured}}$ values measured at
 614 the end of imbibition without enhancement were lower than during the thermal enhancement
 615 experiments: 63 $\Omega\cdot\text{m}$ (vs. 150 $\Omega\cdot\text{m}$ without thermal enhancement) for the 0.5 mm GB and 87 $\Omega\cdot\text{m}$ (vs.
 616 1061 $\Omega\cdot\text{m}$ without thermal enhancement) for the 0.1 mm GB. At the end of imbibition 1, the $\rho_{c,\text{estimated}}$
 617 were respectively 84 $\Omega\cdot\text{m}$ for 0.5 mm GB (vs. 152 $\Omega\cdot\text{m}$ at 20 $^{\circ}\text{C}$) and 112 $\Omega\cdot\text{m}$ for 0.1 mm GB (vs.
 618 203 $\Omega\cdot\text{m}$ at 20 $^{\circ}\text{C}$). In theory, the $\rho_{c,\text{measured}}$ therefore decreased by 45% in both cases.

619

620 4.6 Monitoring of the drainage-imbibition experiments with image interpretation

621 Figure 8 shows an experiment with 0.5 mm GB. The pollutant was dark brown-black. Note that
 622 during the drainage, the migration front was relatively sharp (which corresponded to curve $P_c = f(S_w)$)

623 for drainage 1 with a relatively horizontal plateau – Figure 2). At the end of drainage, the cell was
624 filled with DNAPL but filling was not totally homogeneous (due to wall effects). During the
625 imbibition, the migration front was more diffuse, which was expected considering the $P_c = f(S_w)$ curve
626 for imbibition (which shows a less horizontal pseudo-plateau).

627 Figure A-8 (Supplementary materials) describes the variations of mean grey values for an
628 increasing AOI that begins at the centre of the picture, as detailed below. Increasing the AOI length
629 increased the number of contained pixels. This curve was calculated with a Fiji macro which served to
630 associate a mean grey value with the S_w value, as the grey value was sensitive to the number of pixels
631 inside the selected AOI. However, for AOI between 500 pixels and 1000 pixels, the computed mean
632 grey values were stable, implying that between 2.5×10^5 and 1.0×10^6 pixels were necessary. This
633 interval length was chosen to compute all mean grey values for the calibration curve shown in Figure
634 9.

635 The calibration curve could only be made for the points corresponding to $S_w = 1, 0, S_m$ and S_{rw} . The
636 curve shows a good correlation ($R^2 = 0.98$). The size of the GB did not influence the calibration curve.
637 Also, no differences were observed in Optical Density (OD) measured for $S_w = 1$ and $S_w = 0$. S_m (with
638 respective means of 0.24 and 0.32 for 0.5 and 0.1 mm GB) and S_{rw} values (with respective means of
639 0.89 and 0.84 for 0.5 and 0.1 mm GB) were very close to those measured with the circular 1D cells
640 (less than 3% difference). Variations in S_m and S_{rw} follow a linear regression which is in agreement
641 with the literature [Schincariol et al. (1993); Flores et al. (2011); Watson et al. (2019)]. The optical
642 density experiments show that residual saturations can be estimated accurately ($R^2 = 0.98$) even with
643 surfactants and thermal enhancement. The OD was found to vary linearly as a function of S_w .

644

645 5. Conclusions

646 Drainage-imbibition experiments were performed in 1D cells with the aim of comparing the
647 efficiency of thermal and chemical enhancements on the DNAPL recovery performance. Four
648 different surfactants (SDBS, Aerosol MA-80, Triton X-100 and Tween 80) were tested at
649 concentrations well below their respective CMC (in order to avoid DNAPL dissolution). The best
650 remediation enhancement yield was obtained with SDBS: 27.6% for the 0.5 mm GB and 46.3% for 0.1

651 mm GB. Experiments with thermal enhancement were also conducted at 50 °C (in order to avoid
652 DNAPL volatilization). However, no significant improvement in the remediation enhancement yield
653 was observed.

654 The drainage-imbibition experiments were monitored by electrical resistivity, permittivity and
655 optical density. The goal was to confirm whether the residual saturations could be estimated indirectly.
656 Regarding the permittivity measurements, the estimation of residual saturations fits well with the
657 CRIM model in most cases. The experiments with surfactants and thermal enhancement showed that
658 the variations in residual saturations could also be quantified with permittivity measurements. An
659 adapted version of Archie's Law was used to model resistivity variations as a function of residual
660 saturation variations. The estimated electrical resistivity data showed less correlation with the
661 measurements than the permittivity data. Also, it was not possible to accurately quantify water
662 saturations with electrical resistivity monitoring. However, the accuracy is sufficient (especially for
663 high values of water saturation) for highlighting differences between the treatment technologies. The
664 optical density experiments showed that residual saturations can be accurately estimated even with
665 surfactant and thermal enhancement.

666 Future work will focus on multiphase flow modeling and pumping experiments in a 2 D tank at the
667 laboratory scale, for the purpose of process up-scaling. The permittivity and resistivity measurements
668 as well as the optical densities during the pumping test over time shall provide information regarding
669 how chemical enhancement affects DNAPL recovery yields (at different flow rates). At field scale, the
670 combined monitoring of electrical resistivities (which provide a global picture) and permittivities
671 (which provide accurate but spatially limited information) is expected to improve the reliability of
672 residual saturation data.

673

674 **Acknowledgments**

675 This research was carried out as part of the SILPHES project cofunded by ADEME (French
676 Environment and Energy Management Agency) in the framework of the Future Investments
677 ("Investissements d'Avenir") funding scheme and the BRGM MULTISCALEXPER project. The
678 authors acknowledge ADEME and the BRGM/DEPA division for its financial support. The authors

679 also gratefully acknowledge the financial support provided to the PIVOTS project by the Centre – Val
680 de Loire region (ARD 2020 program and CPER 2015-2020) and the French Ministry of Higher
681 Education and Research (CPER 2015-2020 and public service subsidy to BRGM). Support from the
682 European Union via the European Regional Development Fund is also acknowledged. We thank
683 Florence Rouyer (Laboratoire Navier, Université Paris-Est) for the interfacial tension and contact
684 angle measurements, and INOVYN for the assistance provided during the SILPHES project, in
685 particular for providing access to the Tavaux site and for the dissolved phase analyses.

686

687

688

689 [ADEME and Ernst & Young (2014)] ADEME and Ernst & Young: 2014, *Taux d'utilisation et coûts*
690 *des différentes techniques et filières de traitement des sols et des eaux souterraines polluées en France*
691 – *Synthèse des données 2012*, ADEME edn, Agence de l'Environnement et de la Maîtrise de
692 l'Energie, Agence de l'Environnement et de la Maîtrise de l'Energie - 20, avenue du Grésillé – BP
693 90406 – 49004 Angers Cedex 01. 148 p.

694 [Ahn et al. (2008)] Ahn, C., Kim, Y., Woo, S. and Park, J.: 2008, Soil washing using various
695 nonionic surfactants and their recovery by selective adsorption with activated carbon, *Journal of*
696 *Hazardous Materials* **154**(1–3), 153–160.

697 [Ajo-Franklin et al. (2004)] Ajo-Franklin, J., Geller, J. and Harris, J.: 2004, The dielectric
698 properties of granular media saturated with DNAPL/water mixtures, *Geophysical Research Letters*
699 **31**(L17501), 1–4.

700 [Ajo-Franklin et al. (2006)] Ajo-Franklin, J., Geller, J. and Harris, J.: 2006, A survey of the
701 geophysical properties of chlorinated DNAPLs, *Journal of Applied Geophysics* **59**, 177–189.

702 [Alazaiza et al. (2016)] Alazaiza, M., Nigien, S., Ishak, W. and Kamaruddin, S.: 2016, A review of
703 light reflection and transmission methods in monitoring non-aqueous phase liquid migration in porous
704 media, *Journal of Engineering and Applied Sciences* **11**(4), 2319–2326.

705 [Amirpour et al. (2015)] Amirpour, M., Shadizadeh, S., Esfandyari, H. and Ahmadi, S.: 2015,
706 Experimental investigation of wettability alteration on residual oil saturation using nonionic
707 surfactants: Capillary pressure measurement, *Petroleum* **1**(4), 289–299.

708 [Andersson et al. (2014)] Andersson, M., Bennetzen, M., Klamt, A. and Stipp, S.: 2014, First-
709 Principles Prediction of Liquid/Liquid Interfacial Tension, *Journal of Chemical Theory and*
710 *Computation* **10**, 3401–3408.

711 [Archie (1942)] Archie, G.: 1942, The electrical resistivity log as an aid in determining some reservoir
712 characteristics, *Petroleum Transactions of AIME* **146**(1), 54–62.

713 [Atteia et al. (2013)] Atteia, O., Del Campo Estrada, E. and Bertin, H.: 2013, Soil flushing: a
714 review of the origin of efficiency variability, *Reviews in Environmental Science and Bio/Technology*
715 **12**, 379–389.

716 [Berglund and Cvetkovic (1995)] Berglund, S. and Cvetkovic, V.: 1995, Pump-and-Treat
717 Remediation of Heterogeneous Aquifers: Effects of Rate-Limited Mass Transfer, *Groundwater*
718 **33**, 675–685.

719 [Bernabé et al. (2016)] Bernabé, Y., Li, M., Tang, Y. and Evans, B.: 2016, Pore space connectivity
720 and the transport properties of rocks, *Oil & Gas Science and Technology* **71**(4), 1–17.

721 [Bernabé et al. (2011)] Bernabé, Y., Zamora, M., Li, M., Mainault, A. and Tang, Y.: 2011, Pore
722 connectivity, permeability, and electrical formation factor: A new model and comparison to
723 experimental data, *Journal of Geophysical Research* **116**(B11204), 1–15.

724 [Birchak et al. (1974)] Birchak, J., Gardner, C., Hipp, J. and Victor, J.: 1974, High dielectric constant
725 microwave probes for sensing soil moisture, *Proceedings of the Institute of Electrical and Electronics*
726 *Engineers* **62**(1), 93–98.

727 [Brewster et al. (1995)] Brewster, M., Annan, A., Greenhouse, J., Kueper, B., Olhoeft, G., Redman, J.
728 and Sander, K.: 1995, Observed migration of a controlled DNAPL release by geophysical methods,
729 *Ground Water* **33**, 987–997.

730 [Brovelli and Cassiani (2010)] Brovelli, A. and Cassiani, G.: 2010, A combination of the hashin-
731 shtrikman bounds aimed at modelling electrical conductivity and permittivity of variably saturated
732 porous media, *Geophysical Journal International* **180**, 225–237.

733 [Byun et al. (2019)] Byun, Y., Hong, W. and Yoon, H.: 2019, Characterization of cementation
734 factor of unconsolidated granular materials through time domain reflectometry with variable saturated
735 conditions, *Materials* **12**(8), 1340–1354.

736 [Cai et al. (2017)] Cai, J., Wei, W., Hu, X. and Wood, D.: 2017, Electrical conductivity models
737 in saturated porous media: A review, *Earth-Science Reviews* **171**, 419–433.

738 [Capparelli et al. (2018)] Capparelli, G., Spolverino, G. and Greco, R.: 2018, Experimental
739 Determination of TDR Calibration Relationship for Pyroclastic Ashes of Campania (Italy), *Sensors*
740 **18**(3727), 1–14.

741 [Cazaux et al. (2014)] Cazaux, D., Colombano, S., Joubert, A., Dumestre, A. and Lecuelle, G.: 2014,
742 Optimized physical recovery of DNAPL using upwelling technique and geostatistical analysis at large

743 field scale, *Ninth International Conference on Remediation of Chlorinated and Recalcitrant*
744 *Compounds*, number A1, Battelle Press, Columbus, OH, USA, Monterey, CA, USA, p. 5.

745 [Chambers et al. (2004)] Chambers, J., Loke, M., Ogilvy, R. and Meldrum, P.: 2004,
746 Noninvasive monitoring of DNAPL migration through a saturated porous medium using electrical
747 impedance tomography, *Journal of Contaminant Hydrology* **68**(1–2), 1–22.

748 [Chapuis et al. (2015)] Chapuis, R., Weber, S. and Duhaime, F.: 2015, Permeability test results with
749 packed spheres and non-plastic soils, *Geotechnical Testing Journal* **38**(6), 950–964.

750 [Chiapponi (2017)] Chiapponi, L.: 2017, Water retention curves of multicomponent mixtures of
751 spherical particles, *Powder Technology* **320**, 646–655.

752 [Childs et al. (2004)] Childs, J., Acosta, E., Knox, R., Harwell, J. and Sabatini, D.: 2004, Improving
753 the extraction of tetrachloroethylene from soil columns using surfactant gradient systems, *Journal of*
754 *Contaminant Hydrology* **71**(1-4), 27–45.

755 [Cohen and Mercer (1993)] Cohen, R. and Mercer, J.: 1993, DNAPL Site Evaluation, *Technical*
756 *Report EPA/600/R-93/022*, Edited by USEPA Office of Research and Development. 369 p.

757 [Constable and Srnka (2007)] Constable, S. and Srnka, L.: 2007, An introduction to marine
758 controlled-source electromagnetic methods for hydrocarbon exploration, *Geophysics* **72**(2), WA3–
759 WA12.

760 [Corradini et al. (1996)] Corradini, F., Marchetti, A., Tagliazucchi, M. and Tassi, L.: 1996, Static
761 dielectric constants of 1,2-dichloroethane + 2-methoxyethanol + 1,2-dimethoxyethane ternary liquid
762 mixtures from 10 to 80 °C, *Fluid Phase Equilibria* **124**(1-2), 209– 220.

763 [Dahlin (2000)] Dahlin, T.: 2000, Short note on electrode charge-up effects in dc resistivity data
764 acquisition using multielectrode arrays, *Geophysical Prospecting* **48**(1), 181–187.

765 [Dakhnov (1962)] Dakhnov, V.: 1962, *Geophysical well logging*, number 57-2, Q. Colorado
766 School of Mines. 445 p.

767 [Dasberg and Hopmans (1992)] Dasberg, S. and Hopmans, J.: 1992, Time domain reflectometry
768 calibration for uniformly and nonuniformly wetted sandy and clayey loam soils, *Soil Science Society*
769 *of America Journal* **56**(5), 1341–1345.

770 [Davis (1997)] Davis, E.: 1997, How Heat Can Enhance In-situ Soil and Aquifer
771 Remediation: Important Chemical Properties and Guidance on Choosing the Appropriate Technique,
772 *Technical Report EPA/540/S-97/502*, U.S. Environmental Protection Agency, U.S. Environmental
773 Protection Agency; Solid Waste and Emergency Response, Washington, DC, USA. 18 p.

774 [Deparis et al. (2019)] Deparis, J., Joubert, A., Francois, B., Nodot, E., Invernizzi, T., Iravani, A.,
775 Dumestre, A., Fatin-Rouge, N., Maire, J., Kaifas, D., Triger, A., Klein, P., Giraud, Q., Paris, B.,
776 Cazaux, D., Gourry, J., Davarzani, H. and Colombano, S.: 2019, On the use of Geophysical
777 measurements to monitor DNAPL extraction, *AquaConSoil 2019, 15th International Conference*,
778 Antwerp, Belgium.

779 [Dirksen and Dasberg (1993)] Dirksen, C. and Dasberg, S.: 1993, Improved calibration of time
780 domain reflectometry soil water content measurements, *Soil Science Society of America Journal*
781 **57**(3), 660–667.

782 [Dobson et al. (1985)] Dobson, M., Ulaby, F., Hallikainen, M. and El-Rayes, M.: 1985, Microwave
783 dielectric behaviour of wet soil, part ii, dielectric mixing models, *Institute of Electrical and*
784 *Electronics Engineers Transactions on Geoscience and Remote Sensing* **23**, 35–46.

785 [Duffield and Ramamurthy (2003)] Duffield, A. and Ramamurthy, R.: 2003, Surfactant Enhanced
786 Mobilization of Mineral Oil within Porous Media, *Water, Air, and Soil Pollution* **143**(1–4), 111–122.

787 [Dullien (1992)] Dullien, F.: 1992, *Porous Media: Fluid Transport and Pore Structure*, number
788 978-0-12-223651-8, 2nd edn, Academic Press, San Diego, CA, USA. 574 p.

789 [Dwarakanath et al. (1999)] Dwarakanath, V., Kostarelos, K., Pope, G., Shotts, G. and Wade, W.:
790 1999, Anionic surfactant remediation of soil columns contaminated by nonaqueous phase liquids,
791 *Journal of Contaminant Hydrology* **38**(4), 465–488.

792 [Endres and Knight (1992)] Endres, A. and Knight, R.: 1992, A theoretical treatment of the effect
793 of microscopic fluid distribution on the dielectric properties of partially saturated rocks, *Geophysical*
794 *Prospecting* **40**(3), 307–324.

795 [Falta et al. (2005b)] Falta, R., Basu, N. and Rao, P.: 2005b, Assessing impacts of partial mass
796 depletion in DNAPL source zones: II. Coupling source strength functions to plume evolution, *Journal*
797 *of Contaminant Hydrology* **79**(1-2), 45–66.

798 [Falta et al. (2005a)] Falta, R., Rao, P. and Basu, N.: 2005a, Assessing the impacts of partial mass
799 depletion in DNAPL source zones: I. Analytical modeling of source strength functions and plume
800 response, *Journal of Contaminant Hydrology* **78**(4.), 259–280.

801 [Flores et al. (2011)] Flores, G., Katsumi, T., Inui, T. and Kamon, M.: 2011, A simplified image
802 analysis method to study LNAPL migration in porous media, soils and foundations, *Soils and*
803 *Foundations* **51**(5), 35–847.

804 [Gerhard and Kueper (2003a)] Gerhard, J. and Kueper, B.: 2003a, Capillary pressure characteristics
805 necessary for simulating DNAPL infiltration, redistribution, and immobilization in saturated porous
806 media, *Water Resources Research* **39**(8), 1–17.

807 [Ghanbarian and Sahimi (2017)] Ghanbarian, B. and Sahimi, M.: 2017, Electrical conductivity
808 of partially saturated packings of particles, *Transport in Porous Media* **118**(1), 1–16.

809 [Glover (2010)] Glover, P.: 2010, A generalised archie’s law for n phases, *Geophysics* **6**, E247–E265.

810 [Grellier et al. (2008)] Grellier, S., Guérin, R., Robain, H., Bobachev, A., Vermeersch, F. and
811 Tabbagh, A.: 2008, Monitoring of leachate recirculation in a bioreactor landfill by 2-d electrical
812 resistivity imaging, *Journal of Environmental and Engineering Geophysics* **13**(4), 351–359.

813 [Han et al. (2015)] Han, T., Best, A., Sothcott, J., North, L. and MacGregor, L.: 2015,
814 Relationships among low frequency (2 Hz) electrical resistivity, porosity, clay content and
815 permeability in reservoir sandstones, *Journal of Applied Geophysics* **112**, 279–289.

816 [Harendra and Vipulanandan (2011)] Harendra, S. and Vipulanandan, C.: 2011, Solubilization and
817 degradation of perchloroethylene (PCE) in cationic and nonionic surfactant solutions, *Journal of*
818 *Environmental Sciences* **23**(8), 1240–1248.

819 [Harkness and Konzuk (2014)] Harkness, M. and Konzuk, J.: 2014, *Cost analyses for remedial*
820 *options, in Chapter 16 in Chlorinated Solvent Source Zone Remediation*, number 978-1-4614-6921-6,
821 Springer, SERDP ESTCP Environmental Remediation Technology, New York, NY, USA. 713 p.

822 [Hayashi (2004)] Hayashi, M.: 2004, Temperature-electrical conductivity relation of water for
823 environmental monitoring and geophysical data inversion, *Environmental Monitoring and Assessment*
824 **96**(1-3), 119–128.

825 [Huang et al. (2015)] Huang, J., Christ, J., Goltz, M. and Demond, A.: 2015, Modeling NAPL
826 dissolution from pendular rings in idealized porous media, *Water Resources Research* **51**, 8182–8197.

827 [IARC (2018)] IARC: 2018. <https://www.iarc.fr/>

828 [ITRC (2002)] ITRC: 2002, *DNAPL Source Reduction: Facing the Challenge*, Technical/Regulatory
829 Guidelines, Interstate Technology & Regulatory Council, Washington, DC, USA. 40 p.

830 [Jafvert (1994)] Jafvert, C.: 1994, Solubilization of non-polar compounds by non-ionic surfactant
831 micelles, *Water Research* **28**(5), 1009–1017.

832 [Kargas and Soulis (2012)] Kargas, G. and Soulis, K.: 2012, Performance analysis and calibration
833 of a new low-cost capacitance soil moisture sensor, *Journal of Irrigation and Drainage Engineering*
834 **138**(7), 632–641.

835 [Kommalapati et al. (1997)] Kommalapati, R., Valsaraj, K., Constant, W. and Roy, D.: 1997,
836 Aqueous solubility enhancement and desorption of hexachlorobenzene from soil using a plant-based
837 surfactant, *Water Research* **31**(9), 2161–2170.

838 [Kong (2004)] Kong, L.: 2004, *Characterization of mineral oil, coal tar and soil properties and*
839 *investigation of mechanisms that affect coal tar entrapment in and removal from porous media*, PhD
840 thesis, School of Civil and Environmental Engineering, Georgia Institute of Technology, Atlanta,
841 Atlanta, GA, USA. 309 p. <https://smartech.gatech.edu/handle/1853/5093?show=full>

842 [Kueper et al. (1993)] Kueper, B., Redman, D., Starr, R., Reitsma, S. and Mah, M.: 1993, A field
843 experiment to study the behavior of tetrachlorethylene below the water table: Spatial distribution of
844 residual and pooled DNAPL, *Ground Water* **31**, 756– 766.

845 [Kueper et al. (2003)] Kueper, B., Wealthall, G., Smith, J., Leharne, S. and Lerner, D.: 2003, *An*
846 *illustrated handbook of DNAPL transport and fate in the subsurface*, number 1844320669, U.K.
847 Environment Agency, Bristol, England, United Kingdom. 67 p.

848 [Lake (1989)] Lake, L.: 1989, *Enhanced Oil Recovery*, number 0132816016 9780132816014,
849 Prentice Hall, Old Tappan, NJ, USA. 550 p.

850 [Lenormand et al. (1988)] Lenormand, R., Touboul, E. and Zarcone, C.: 1988, Numerical models
851 and experiments on immiscible displacements in porous media, *Journal of Fluid Mechanics* **189**, 165–
852 187.

853 [Li et al. (2015)] Li, M., Tang, Y., Bernabé, Y., Zhao, J., Li, X., Bai, X. and Zhang, L.: 2015,
854 Pore connectivity, electrical conductivity, and partial water saturation: Network simulations, *Journal*
855 *of Geophysical Research: Solid Earth* **120**(6), 4055–4068.

856 [Light et al. (2005)] Light, T., Licht, S., Bevilacqua, A. and Morashc, K.: 2005, The fundamental
857 conductivity and resistivity of water, *Electrochemical and Solid-State Letters* **8**(1), E16–E19.

858 [Likos and Jaafar (2013)] Likos, W. and Jaafar, R.: 2013, Pore-scale model for water retention
859 and fluid partitioning of partially saturated granular soil, *Journal of Geotechnical and*
860 *Geoenvironmental Engineering* **139**(5), 724–737.

861 [Logsdon (2000)] Logsdon, S.: 2000, Effect of cable length on time domain reflectometry
862 calibration for high surface area soils, *Soil Science Society of America Journal* **64**(1), 54–61.

863 [Logsdon (2005)] Logsdon, S.: 2005, Soil dielectric spectra from vector network analyzer data,
864 *Soil Science Society of America Journal* **69**(4), 983–989.

865 [Loon et al. (1967)] Loon, R., Fuks, S. and Bellemans, A.: 1967, Dielectric constant of carbon
866 tetrachloride and 1,1,1-trichloroethane mixtures, *Bulletin des Societes Chimiques Belges* **76**(3-4), 202–
867 210.

868 [Luciano et al. (2010)] Luciano, A., Viotti, P. and Papini, M. P.: 2010, Laboratory investigation of
869 DNAPL migration in porous media, *Journal of Hazardous Materials* **176**(1-3), 1006–1017.

870 [Mackay and Cherry (1989)] Mackay, D. and Cherry, J.: 1989, Groundwater contamination: pump-
871 and-treat remediation, *Environmental Science & Technology* **23**, 630–636.

872 [Maire et al. (2018)] Maire, J., Joubert, A., Kaifas, D., Invernizzi, T., Mardue, J., Colombano, S.,
873 Cazaux, D., Marion, C., Klein, P., Dumestre, A. and Fatin-Rouge, N.: 2018, Assessment of flushing
874 methods for the removal of heavy chlorinated compounds DNAPL in an alluvial aquifer, *Science of*
875 *the Total Environment* (612), 1149–1158.

876 [McDade et al. (2005)] McDade, J., McGuire, T. and Newell, C.: 2005, Analysis of DNAPL source-
877 depletion costs at 36 field sites, *Remediation Journal* **15**(2:), 9–18.

878 [McGuire et al. (2006)] McGuire, T., McDade, J. and Newell, C.: 2006, Performance of DNAPL
879 Source Depletion Technologies at 59 Chlorinated Solvent-Impacted Sites, *Ground Water Monitoring*
880 *and Remediation* **26**(1), 73–84.

881 [Morgan and Lowry (1930)] Morgan, S. and Lowry, H.: 1930, Dielectric polarization of some pure
882 organic compounds in the dissolved, liquid, and solid states, *The Journal of Physical Chemistry*
883 **34**(11), 2385–2432.

884 [Mualem (1976)] Mualem, Y.: 1976, A new model for predicting the hydraulic conductivity of
885 unsaturated porous media, *Water Resources Research* **12**(3), 513–522.

886 [Nath (1995)] Nath, J.: 1995, Ultrasonic velocities, relative permittivities, and refractive indices for
887 binary liquid mixtures of trichloroethylene with pyridine and quinoline, *Fluid Phase Equilibria*
888 **109**(1), 39–51.

889 [Nath and Narain (1982)] Nath, J. and Narain, B.: 1982, Binary systems of tetrachlorethylene
890 with benzene, toluence, p-xylene, carbon tetrachloride, and cyclohexane. 1. Ultrasonic velocities and
891 adiabatic compressibilities at 293.15 and 303.15 K, dielectric constants at 298.15 and 308.15 K, and
892 refractive indexes at 298.15 K, *Journal of Chemical Engineering Data* **27**(3), 308–312.

893 [Newell and Adamson (2005)] Newell, C. and Adamson, D.: 2005, Planning-level source decay
894 models to evaluate impact of source depletion on remediation timeframe, *Remediation* **15**(4), 27–47.

895 [NIEHS (2015)] NIEHS: 2015, Chlorinated organics – information page, website.
896 http://tools.niehs.nih.gov/srp/research/research4_s3_s4.cfm

897 [Noel (2014)] Noel, C.: 2014, *Suivi de la biodégradation des hydrocarbures par le couplage des*
898 *mesures géophysiques électriques du sol (polarisation provoquée) et des analyses des gaz*
899 *(concentration du CO₂ et isotopie du carbone)*, PhD thesis, Université d’Orléans, Orléans, France.
900 256 p.

901 [O’Carroll et al. (2004)] O’Carroll, D., Bradford, S. and Abriola, L.: 2004, Infiltration of PCE
902 in a system containing spatial wettability variations, *Journal of Contaminant Hydrology* **73**(1-4), 39–
903 63.

904 [Orphius and Kibbey (2005)] Orphius, I. and Kibbey, T.: 2005, Dissolution-Induced Contact Angle
905 Modification in Dense Nonaqueous Phase Liquid (DNAPL)/Water Systems, *Environmental Science*
906 *and Technology* **39**, 1698–1706.

907 [Ouchiyama and Tanaka (1984)] Ouchiyama, N. and Tanaka, T.: 1984, Porosity estimation for
908 random packings of spherical particles, *Industrial & Engineering Chemistry Fundamentals* **23**, 490–
909 493.

910 [Pankow and Cherry (1996)] Pankow, J. and Cherry, J.: 1996, *Dense Chlorinated Solvents and*
911 *Other DNAPLs in Groundwater: History, Behavior, and Remediation*, number 978-0964801417,
912 Waterloo Press, Portland, OR, USA. 525 p.

913 [Pennell et al. (2014)] Pennell, K., Capiro, N. and Walker, D.: 2014, *Surfactant and cosolvent*
914 *flushing, Chapter 11 in Chlorinated Solvent Source Zone Remediation*, number 978-1-4614-6921-6,
915 Springer, SERDP ESTCP Environmental Remediation Technology, New York, NY, USA. 713 p.

916 [Pennell et al. (1996)] Pennell, K., Pope, G. and Abriola, L.: 1996, Influence of viscous and
917 buoyancy forces on the mobilization of residual tetrachloroethylene during surfactant flushing,
918 *Environmental Science & Technology* **30**, 1328–1335.

919 [Persson and Berndtsson (1998)] Persson, M. and Berndtsson, R.: 1998, Texture and electrical
920 conductivity effects on temperature dependency in time domain reflectometry, *Soil Science Society of*
921 *America Journal* **62**(4), 887–893.

922 [Persson and Berndtsson (2002)] Persson, M. and Berndtsson, R.: 2002, Measuring nonaqueous
923 phase liquid saturation in soil using time domain reflectometry, *Water Resources Research*
924 **38**(5), 22.1–22.8.

925 [Redman and DeRyck (1994)] Redman, J. and DeRyck, S.: 1994, Monitoring non-aqueous phase
926 liquids in the subsurface with multilevel time domain reflectometry probes, *Proceedings of the*
927 *Symposium on Time Domain Reflectometry in Environmental, Infrastructure, and Mining*
928 *Applications*, Spec. Publ. SP, .NTIS PB95-105789, 19-94, U.S. Bur. of Mines, Washington, D.C.,
929 USA, p. 207– 215.

930 [Redman et al. (1991)] Redman, J., Kueper, B. and Annan, A.: 1991, Dielectric stratigraphy of a
931 DNAPL spill and implications for detection with ground penetrating radar, *Aquifer Restoration,*
932 *Ground Water Monitoring and Geophysical Methods, 5th National Outdoor Action Conference*, Natl.
933 Ground Water Assoc., Las Vegas, NV., USA.

934 [Revil (2012)] Revil, A.: 2012, Spectral induced polarization of shaly sands: influence of the
935 electrical double layer, *Water Resources Research* **48**(2), 1–23.

936 [Reynolds (2011)] Reynolds, J.: 2011, *An Introduction to Applied and Environmental*
937 *Geophysics*, number 978-0-471-48535-3, 2nd edition edn, Wiley-Blackwell, Chichester, UK. 710 p.

938 [Robinson and Friedman (2001)] Robinson, D. and Friedman, S.: 2001, Effect of particle size
939 distribution on the effective dielectric permittivity of saturated granular media, *Water Resources*
940 *Research* **37**(1), 33–40.

941 [Robinson and Friedman (2002)] Robinson, D. and Friedman, S.: 2002, The effective
942 permittivity of dense packings of glass beads, quartz sand and their mixtures immersed in different
943 dielectric backgrounds, *Journal of Non-Crystalline Solids* **305**, 261–267.

944 [Robinson et al. (2005)] Robinson, D., Jones, S., Blonquist, J. and Friedman, S.: 2005, A physically
945 derived water content/permittivity calibration model for coarse-textured, layered soils, *Soil Science*
946 *Society of America Journal* **69**(5), 1372.

947 [Rodrigues et al. (2017)] Rodrigues, R., Betelu, S., Colombano, S., Masselot, G., Tzedakis, T.
948 and Ignatiadis, I.: 2017, Influence of temperature and surfactants on the solubilization of
949 hexachlorobutadiene and hexachloroethane, *Journal of Chemical & Engineering Data* **62**(10), 3252–
950 3260.

951 [Rosen (1989)] Rosen, M.: 1989, *Surfactants and Interfacial Phenomena*, 2nd edn, John Wiley and
952 Sons, New York, NY, USA. 431 p.

953 [Roth et al. (1990)] Roth, K., Schulin, R., Fluhler, H. and Attinger, W.: 1990, Calibration of time
954 domain reflectometry for water content measurements using a composite dielectric approach, *Water*
955 *Resources Research* **26**, 2267–2273.

956 [Sabatini et al. (1998)] Sabatini, D., Harwell, J., Hasegawa, M. and Knox, R.: 1998, Membrane
957 processes and surfactant-enhanced subsurface remediation: results of a field demonstration, *Journal of*
958 *Membrane Science* **151**(1), 87–98.

959 [Sabatini et al. (2000)] Sabatini, D., Knox, R., Harwell, J. and Wu, B.: 2000, Integrated design of
960 surfactant enhanced DNAPL remediation: Efficient supersolubilization and gradient systems, *Journal*
961 *of Contaminant Hydrology* **45**(1-2), 99–121.

962 [Sale (2001)] Sale, T.: 2001, Methods for Determining Inputs to Environmental Petroleum
963 Hydrocarbon Mobility and Recovery Models, *Technical Report API PUBLICATION 4711*, American
964 Petroleum Institute, 1220 L Street, Northwest., Washington, DC, USA. 72 p.

965 [Schincariol et al. (1993)] Schincariol, R., Herderick, E. and Schwartz, F.: 1993, On the
966 application of image analysis to determine concentration distributions in laboratory experiments,
967 *Journal of Contaminant Hydrology* **12**(3), 197–215.

968 [Schincariol and Schwartz (1990)] Schincariol, R. and Schwartz, F.: 1990, An experimental
969 investigation of variable density flow and mixing in homogeneous and heterogeneous media, *Water*
970 *Resources Research* **26**(10), 2317–2329.

971 [Schwille (1988)] Schwille, F.: 1988, *Dense Chlorinated Solvents in Porous and Fractured*
972 *Media - Model Experiments*, number 978-0873711210, Lewis Publishers, Chelsea, MI, USA. 146 p.

973 [Seyfried and Grant (2007)] Seyfried, M. and Grant, L.: 2007, Temperature effects on soil
974 dielectric properties measured at 50 mhz, *Vadose Zone Journal* **6**(4), 759–765.

975 [She and Sleep (1998)] She, H. and Sleep, B.: 1998, The effect of temperature on capillary pressure-
976 saturation relationships for air-water and perchloroethylene-water systems, *Water Resources Research*
977 **34**(10), 2587–2597.

978 [Sheng (2015)] Sheng, J.: 2015, Status of surfactant EOR technology, *Petroleum* **1**, 97–105.

979 [Sleep and Ma (1997)] Sleep, B. and Ma, Y.: 1997, Thermal variation of organic fluid properties and
980 impact on thermal remediation feasibility, *Journal of Soil Contamination* **6**(3), 281–306.

981 [Stimson (1974)] Stimson, A.: 1974, *Photometry and Radiometry for Engineers*, number 978-
982 0471825319, John Wiley & Sons Inc, New York, NY, USA. 488 p.

983 [Stroo et al. (2012)] Stroo, H., Leeson, A., Marqusee, J., Johnson, P., Ward, C., Kavanaugh, M.,
984 Sale, T., Newell, C., Pennell, K., Lebrón, C. and Unger, M.: 2012, Chlorinated ethene source
985 remediation: lessons learned, *Environmental Science & Technology* **46**(6438–6447).

986 [Stroo et al. (2003)] Stroo, H., Unger, M., Ward, C., Kavanaugh, M., Vogel, C., Leeson, A.,
987 Marqusee, J. and Smith, B.: 2003, Peer Reviewed: Remediating Chlorinated Solvent Source Zones, A
988 workshop lists the challenges and research needs, *Environmental Science & Technology*
989 **37**(11), 224A–230A.

990 [Stupp and Paus (1999)] Stupp, H. and Paus, L.: 1999, Migrationsverhalten organischer
991 Grundwasser-Inhaltsstoffe und daraus resultierende Ansätze zur Beurteilung von Monitored Natural
992 Attenuation (MNA), *TerraTech* (5).

993 [Suchomel et al. (2007)] Suchomel, E., Ramsburg, C. and Pennell, K.: 2007, Evaluation of
994 trichloroethene recovery processes in heterogeneous aquifer cells flushed with biodegradable
995 surfactants, *Journal of Contaminant Hydrology* **94**(3-4), 195–214.

996 [Taylor et al. (2001)] Taylor, T., Pennell, K., Abriola, L. and Dane, J.: 2001, Surfactant enhanced
997 recovery of tetrachloroethylene from a porous medium containing low permeability lenses: 1.
998 Experimental studies, *Journal of Contaminant Hydrology* **48**(3–4), 325–350.

999 [Travis and Doty (1990)] Travis, C. and Doty, C.: 1990, Can contaminated aquifers at
1000 Superfund sites be remediated?, *Environmental Science & Technology* **24**, 1464–1466.

1001 [van Genuchten (1980)] van Genuchten, M.: 1980, A closed-form equation for predicting the hydraulic
1002 conductivity of unsaturated soils, *Soil Science Society of America* **44**, 892–898.

1003 [von Hippel (1954)] von Hippel, A.: 1954, *Dielectric Materials and Applications*, Technology
1004 Press of M.I.T. and Wiley, Hoboken, N J, USA. 456 p.

1005 [Watson et al. (2019)] Watson, F., Maes, J., Geiger, S., Mackay, E., Singleton, M., McGravie, T.,
1006 Anouilh, T., Jobe, T., Zhang, S., Agar, S., Ishutov, S. and Hasiuk, F.: 2019, Comparison of Flow and
1007 Transport Experiments on 3D Printed Micromodels with Direct Numerical Simulations, *Transport in*
1008 *Porous Media* **129**(2), 449–466.

1009 [Weast (1986)] Weast, R.: 1986, *CRC handbook of chemistry and physics*, 67th edition edn, CRC
1010 Press Inc, Boca Raton, FL, USA. 2424 p.

1011 [Zhao et al. (2006)] Zhao, B., Zhu, L. and Yang, K.: 2006, Solubilization of DNAPLs by mixed
1012 surfactant: Reduction in partitioning losses of nonionic surfactant, *Chemosphere* **62**(5), 772–779.

1013 [Zhong et al. (2003)] Zhong, L., Mayer, A. and Pope, G.: 2003, The effects of surfactant
1014 formulation on nonequilibrium NAPL solubilization, *Journal of Contaminant Hydrology* **60**(1-2), 55–
1015 75.

1016

1017

1018

1019 Figure 1: Schematic of 1D cell

1020 Figure 2: Pressure-water saturation curves for 0.5 and 0.1 mm GB: a) drainage-imbibition without
1021 enhancement and b) imbibition without surfactant and with SDBS

1022 Figure 3: Comparison of a) Capillary number (N_{ca}), b) Bond number (N_B), and c) Total trapping
1023 number (N_T) for 0.5 and 0.1 mm GB

1024 Figure 4: Fitting the experimental permittivity values as function of water saturation with the CRIM
1025 model: a) 0.5 mm GB and b) 0.1 mm GB

1026 Figure 5: Change of water saturation and permittivity (measured and estimated) as a function of
1027 drainage-imbibition cycle for 0.5 and 0.1 mm GB in 1D cells (with and without enhancements)

1028 Figure 6: Fitting the experimental resistivity values as a function of water saturation with Archie's
1029 law: a) 0.5 mm GB and b) 0.1 mm GB

1030 Figure 7: Change of water saturation and resistivity (measured and estimated) as a function of
1031 drainage-imbibition cycle for 0.5 and 0.1 mm GB in 1D cells (with and without enhancements)

1032 Figure 8: Drainage-imbibition experiments in the Hele-Shaw cell (example with 0.5 mm GB)

1033 Figure 9: Fitting the experimental optical density values as a function of water saturation (without
1034 enhancement, with chemical and thermal enhancements)

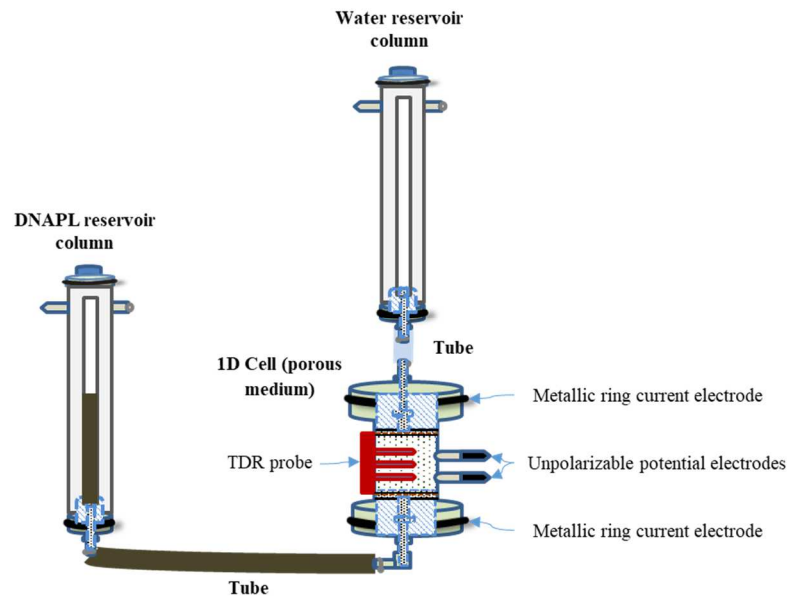
1035 Table 1: Results of drainage-imbibition experiments for 0.5 and 0.1 mm GB

1036

1037

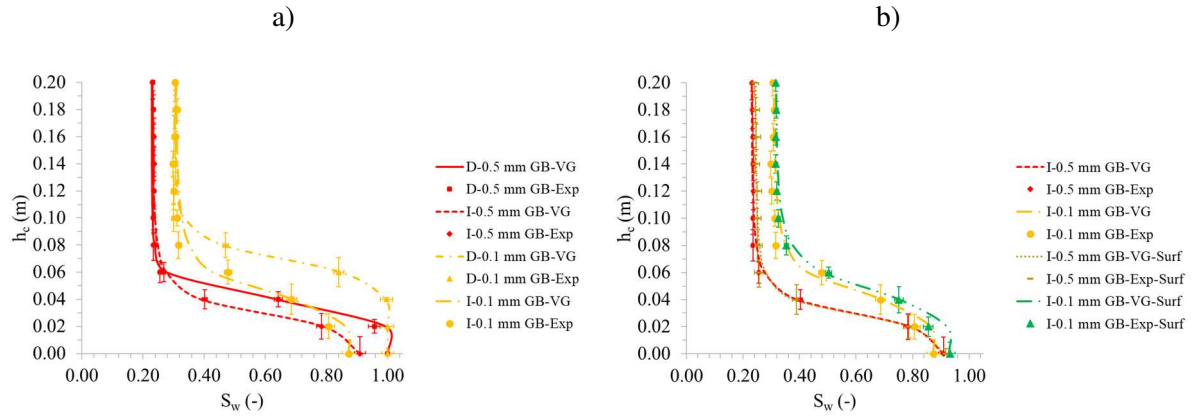
1038

1
2



3
4
5

Figure 1: Schematic of 1D cell

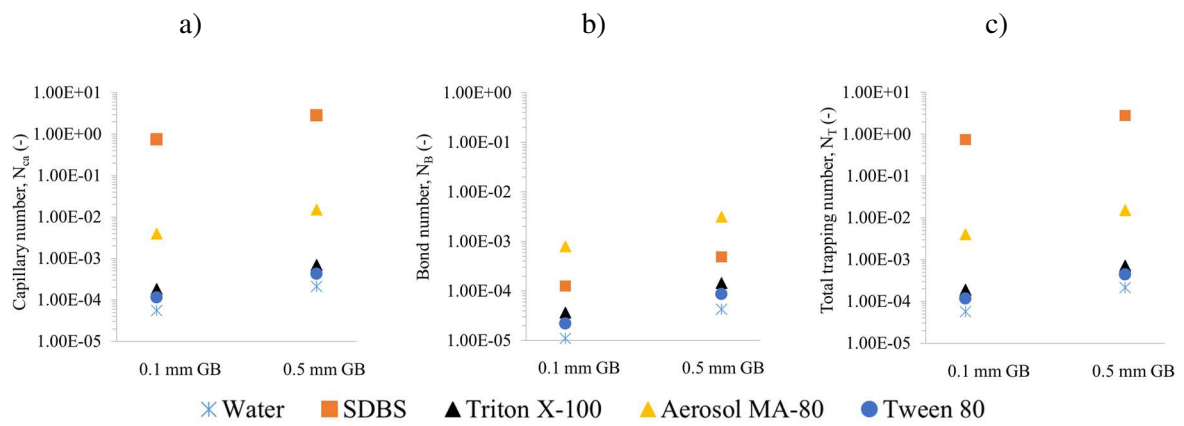


(D: drainage, I: imbibition, VG: Van Genuchten Mualem fitting values; Exp : raw values; Surf: addition of SDBS)

6
7
8
9

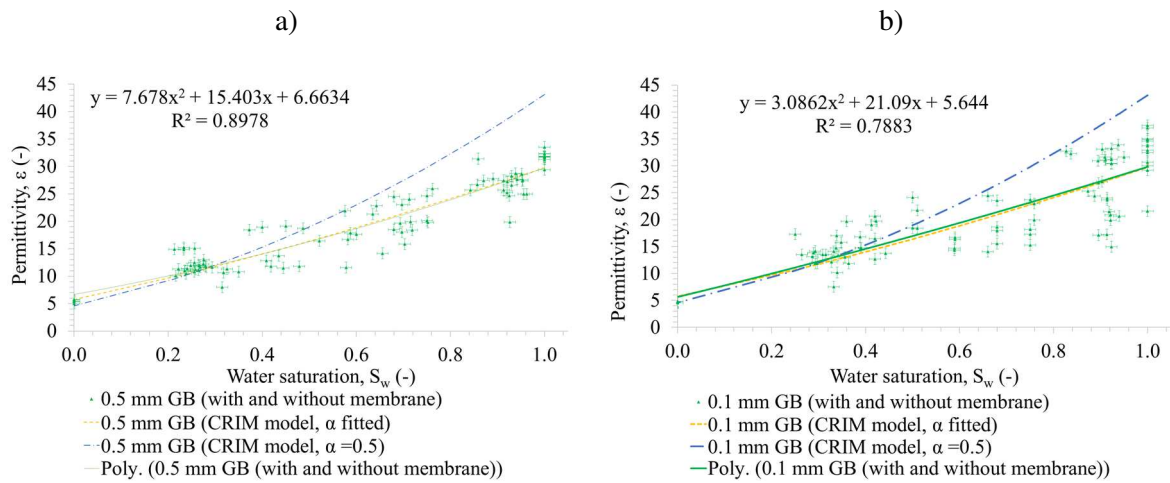
Figure 2: Pressure-water saturation curves for 0.5 and 0.1 mm GB: a) drainage-imbibition without enhancement and b) imbibition without surfactant and with SDBS

10



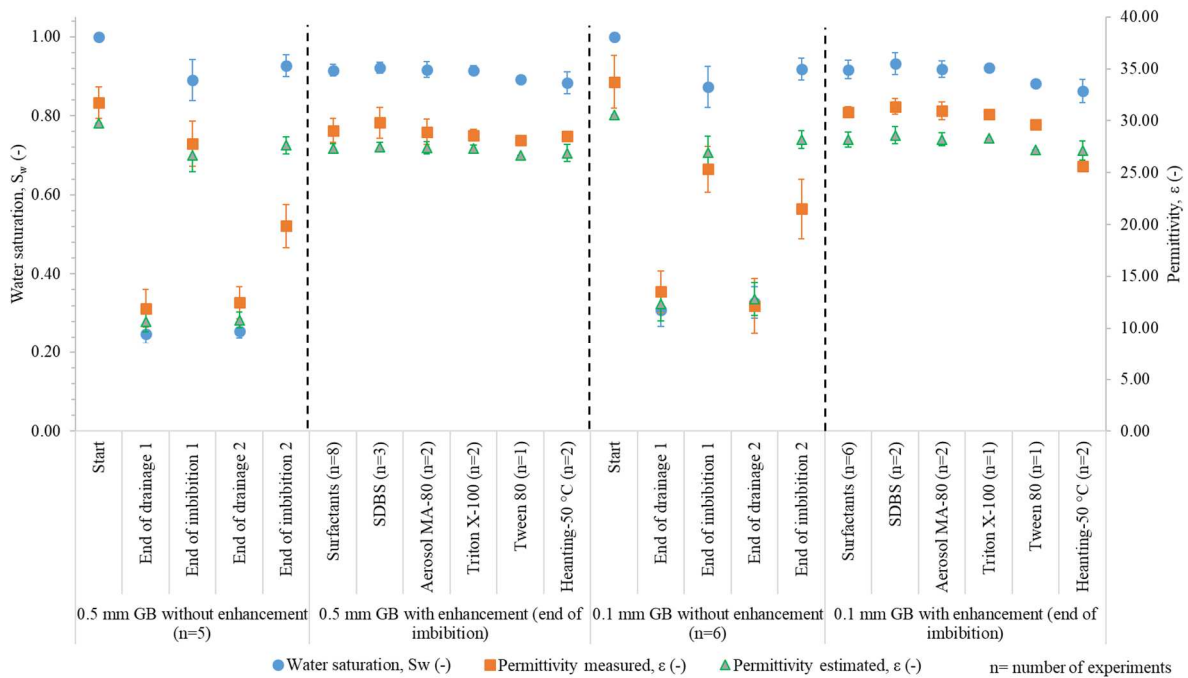
11 Figure 3: Comparison of a) Capillary number (N_{ca}), b) Bond number (N_B), and c) Total trapping
12 number (N_T) for 0.5 and 0.1 mm GB
13
14

15



16 Figure 4: Fitting the experimental permittivity values as function of water saturation with the CRIM
 17 model: a) 0.5 mm GB and b) 0.1 mm GB

18



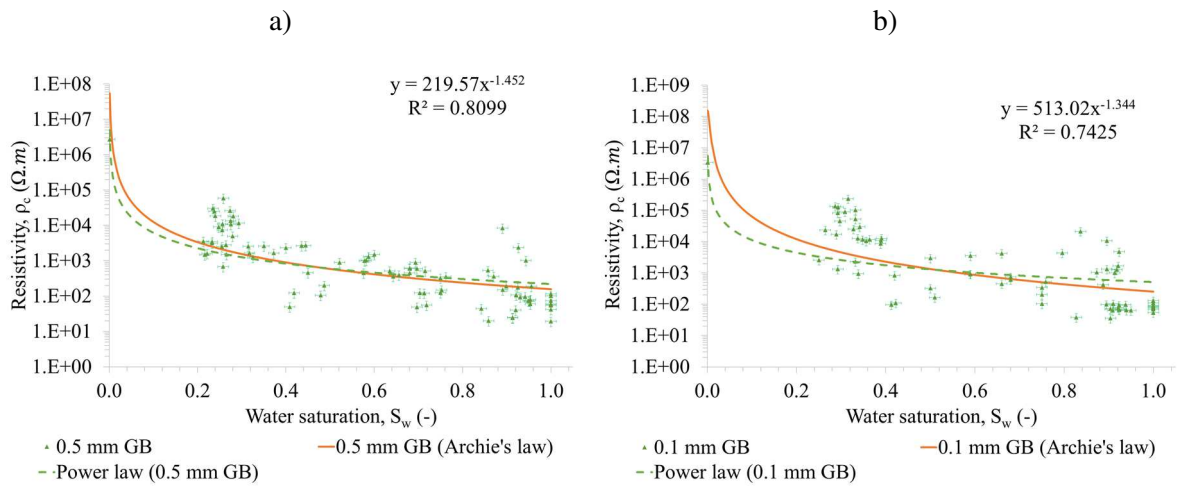
19

20 Figure 5: Change of water saturation and permittivity (measured and estimated) as a function of
 21 drainage-imbibition cycle for 0.5 and 0.1 mm GB in 1D cells (with and without enhancements)

22

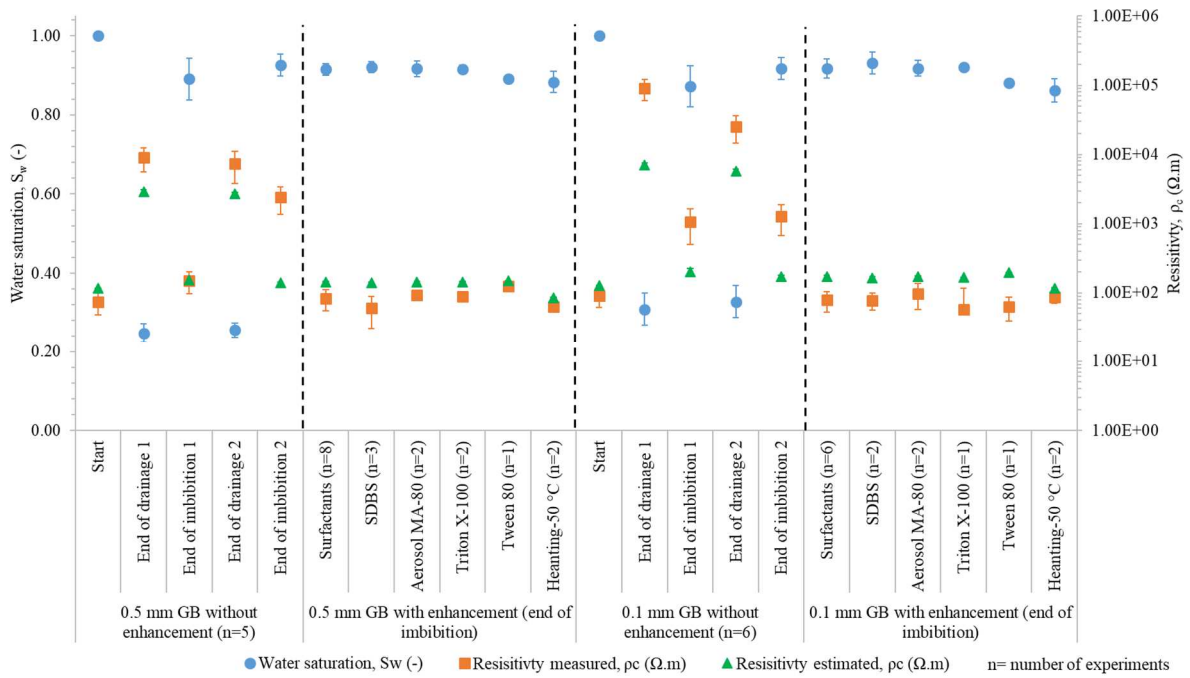
23

24



25 Figure 6: Fitting the experimental resistivity values as a function of water saturation with Archie's
 26 law: a) 0.5 mm GB and b) 0.1 mm GB

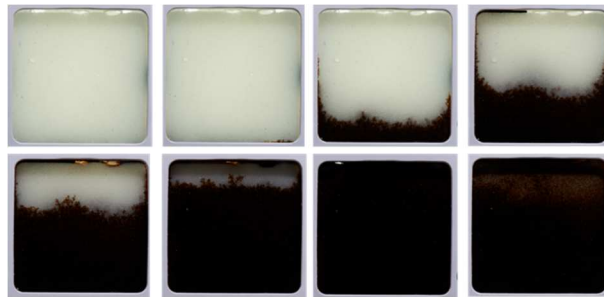
27



28
 29 Figure 7: Change of water saturation and resistivity (measured and estimated) as a function of
 30 drainage-imbibition cycle for 0.5 and 0.1 mm GB in 1D cells (with and without enhancements)

31

Drainage 1



Imbibition 1

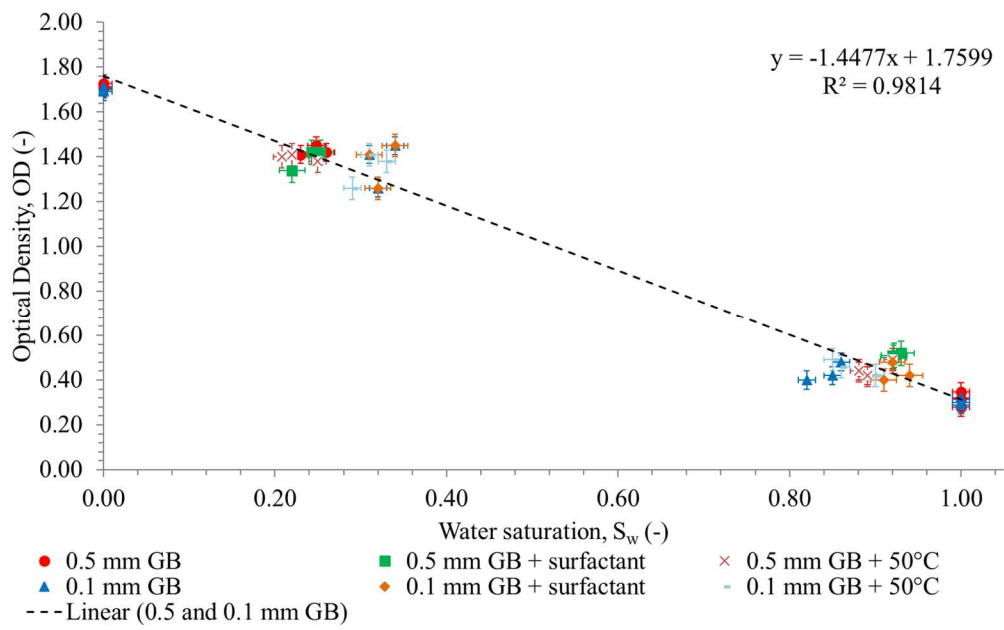


Drainage 2



Figure 8: Drainage-imbibition experiments in the Hele-Shaw cell (example with 0.5 mm GB)

35



36

37 Figure 9: Fitting the experimental optical density values as a function of water saturation (without

38 enhancement, with chemical and thermal enhancements)

39

1

2

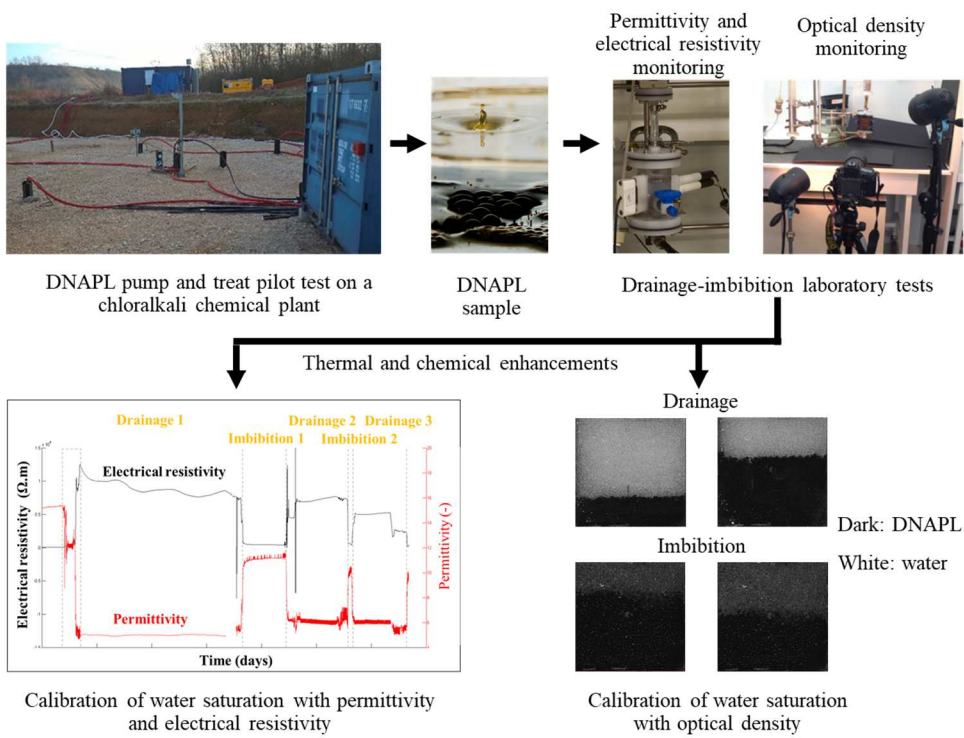
3

Table 1: Results of drainage-imbibition experiments for 0.5 and 0.1 mm GB

Parameters	0.5 mm GB		0.1 mm GB	
	Drainage D	Imbibition I	Drainage D	Imbibition I
α (m ⁻¹)	26.06	38.36	14.72	23.29
n (-)	15.35	5.15	9.49	16.98
SSE	0.0038	0.0025	0.0056	0.0214
S _{rn} (-)	0.000	0.109	0.000	0.127
S _{rw} (-)	0.248	0.248	0.309	0.309

4

1 Graphical abstract



- 2
- 3
- 4